Plant Physiology and Biochemistry 231 (2026) 110981

Contents lists available at ScienceDirect

Plant Physiology and Biochemistry

journal homepage: www.elsevier.com/locate/plaphy

Network-based multiomics and transgenic validation reveal that *OsPHR3* modulates phosphate-carbon metabolic trade-offs during rice seed development

Lekha Pazhamala [a,*], Mandavi Pandey [a], Priyanka Deveshwar [a], Arindam Ghatak [b,c], Wolfram Weckwerth [b,c], Palak Chaturvedi [b], Jitender Giri [a,**]

[a] National Institute of Plant Genome Research (NIPGR), Aruna Asaf Ali Marg, New Delhi, Delhi, 110067, India
[b] Molecular Systems Biology Lab (MOSYS), Department of Functional and Evolutionary Ecology, University of Vienna, Djerassiplatz 1, 1030, Vienna, Austria
[c] Vienna Metabolomics Center, University of Vienna, Djerassiplatz 1, 1030, Vienna, Austria

ARTICLE INFO

Keywords:
Grain filling
Phosphate
Rice
Phytate
Seed development
Os*PHR3*
Multiomics

ABSTRACT

Phosphate (Pi) allocation during the grain-filling stage is a major determinant of crop yield, supporting macromolecule synthesis, energy metabolism, and nutrient storage. However, its storage as phytic acid (PA) reduces nutritional quality by chelating essential minerals. Despite its importance, a comprehensive understanding of the molecular mechanisms integrating Pi transport, carbohydrate metabolism, and PA biosynthesis during seed development remains incomplete. To address this gap, we investigated stage-specific phosphate regulatory networks in rice by integrating transcriptomic, proteomic, and metabolomic approaches. Temporal expression profiling and gene coexpression network analyses of phosphate regulators and transporter genes revealed their distinct roles during early and mid-grain filling stages. *PHOSPHATE STARVATION RESPONSE 3* (*OsPHR3)* emerged as a central regulatory hub, coordinating the balance of Pi, sugar, starch and phytate, along with other metabolites. Network-based multiomics integration further identified 126 genes involved in nutrient storage and stress tolerance, with *myo-inositol-1-phosphate synthase* (*OsMIPS1*) and *starch synthase 3* (*OsSSIII*) as key genes. CRISPR/Cas9-generated *osphr3* knockout lines confirmed the critical role of *OsPHR3* in regulating these target genes. Mutants exhibited significantly reduced seed starch, PA, and total phosphorus contents, while scanning electron microscopy revealed aberrant starch granule morphology. Loss-of-function of *OsPHR3* lowered PA levels by 19.46–22.50 %, with moderate trade-offs in yield-related traits. Although, *OsPHR3* is known to contribute to nitrogen and phosphorus homeostasis, our findings establish it as a key regulator orchestrating a stage-specific phosphate-carbon allocation during seed development. These insights provide key targets for refining nutrient partitioning to achieve increased yields, reduced phytic acid, and enhanced phosphorus use efficiency for agricultural sustainability.

1. Introduction

Rice is the primary source of calories for over 3.5 billion people worldwide (Seck et al., 2012; Fang et al., 2021). To meet the escalating food demand, global rice production must increase by 75 million tons by 2050 (Kruseman et al., 2020). However, cereal productivity is severely constrained by the low bioavailability of soil inorganic phosphate (Pi) (Rose et al., 2013; Cong et al., 2020; Lambers, 2022). Pi is essential for cellular metabolites (ATP, nucleic acids, and phospholipids), and ADP-glucose synthesis during starch accumulation, influencing grain filling. Excess phosphorus (P) accumulates as phytate, the primary seed storage form (Ma et al., 2021; Raboy, 2020). While phytate supports germination, it is indigestible in humans/animals, and interferes with mineral bioavailability due to its strong affinity for iron, zinc, magnesium, calcium, manganese, and cadmium (Rose et al., 2020; Mohammadi et al., 2021). The phytate-derived waste discharged also contributes to environmental issues, such as the eutrophication of water bodies (Lott et al., 2000; Conley et al., 2009; Raboy, 2007, 2009).

* Corresponding author.
** Corresponding author.
E-mail addresses: lekha.pazhamala@gmail.com (L. Pazhamala), jitender@nipgr.ac.in, jitender.giri@gmail.com (J. Giri).

https://doi.org/10.1016/j.plaphy.2025.110981
Received 29 August 2025; Received in revised form 10 December 2025; Accepted 20 December 2025
Available online 22 December 2025

Therefore, reducing grain phytate without compromising seedling vigor offers both nutritional and environmental benefits (Wang et al., 2016).

In cereals, especially rice, the majority of above-ground P is allocated to grains (Raboy, 2001, 2009; Veneklaas et al., 2012; Julia et al., 2016). This active Pi loading into grains results in a higher P harvest index (which exceeds the biomass harvest index), a trait conserved during domestication and breeding programs of major crop species (Rose et al., 2007; Bi et al., 2013). Approximately 80 % of applied phosphorus fertilizer globally is removed from fields during harvest, primarily through cereal grains, the main route of phosphorus export from agricultural fields (Lambers, 2022; Lott et al., 2000; Julia et al., 2016; Tuncel and Okita, 2013; Raboy, 2020). However, phosphorus use efficiency remains low (<20 %) due to soil fixation, limiting crop uptake (Ma et al., 2021; Oldroyd and Leyser, 2020; Pazhamala and Giri, 2023). Consequently, farmers rely heavily on P-based fertilizers derived from nonrenewable phosphate rock, often imported in large quantities in countries like India (Illakwahhi et al., 2024; Poirier et al., 2022). Ensuring sustainable yields with reduced P inputs presents a significant challenge.

Pi acquisition and reallocation are critical processes during the reproductive phase of plants, substantially influencing crop yield (Wang et al., 2021). At maturity, approximately 20 % of the total P in vegetative tissues is remobilized to the panicle, the major P sink. Studies suggest that during grain filling, P uptake relies on stored P within the vegetative tissues (Julia et al., 2016). Various phosphate transporters facilitate this Pi loading by translocating Pi from the vascular bundle located in the nodes near the panicle (Yamaji and Ma, 2014, 2017; Che et al., 2020). In rice, only a few key phosphate-related genes and gene families that control seed development and the grain filling process have been reported recently, including *OsPHO1;2*, a PHO1-type Pi transporter (Ma et al., 2021, 2024; Che et al., 2020; Xu and Yi, 2021; Ko et al., 2024). Recently, frameshift mutations in the *OsIPK1* gene, which encodes Inositol 1,3,4,5,6-pentakisphosphate 2-kinase (IPK1), led to excessive accumulation of Pi, resulting in a decline in starch biosynthesis (Wang et al., 2024). To develop rice varieties with reduced phytate content without compromising the grain filling or seed germination process, understanding the molecular mechanisms and identifying key molecular players that underpin Pi loading and unloading during grain development in rice is a crucial initial step (Vogiatzaki et al., 2017).

The current omics era generates large-scale transcriptome, proteome, and metabolome datasets that are routinely analyzed across multiple plant species (Weckwerth et al., 2020). In this study, transcriptomic data curated from the NCBI SRA database for developing seeds and endosperm in rice were analyzed to identify co-expressed gene clusters and functional groups associated with genes known to regulate Pi acquisition and reallocation during seed development.These transcriptomic insights were further integrated with newly generated proteomic and metabolomic profiles from *Oryza sativa* seeds at early seed development (E), mid-grain filling (M), and late seed maturation (L) stages (Fig. S1a). By adopting a network-based integrated multiomics strategy, we aimed to achieve a system-level understanding of Pi loading and unloading dynamics, and to pinpoint key regulatory genes involved in these processes. Our study is based on the hypothesis that Pi accumulation and mobilization during seed development are highly regulated processes and can be computationally modeled using network biology approaches, as demonstrated in previous studies on rice (Guo et al., 2021), pigeonpea (Pazhamala et al., 2017, 2020), and tomato (Keller et al., 2018) among others. Despite the identification of some candidate genes, the key regulators orchestrating Pi and carbon partitioning during endosperm development remain largely unknown, and the complete regulatory network is yet to be elucidated. This knowledge gap prompted us to undertake a deeper multiomics investigation to uncover the molecular mechanisms and regulatory pathways underlying Pi dynamics during seed development and grain filling.

2. Materials and methods

2.1. Plant material and sample harvest

The Nipponbare genotype of rice was cultivated under controlled field conditions, and seeds were tagged at 0 days after anthesis (DAA) to facilitate the identification of various developmental stages. For this study, seed samples were collected at Early (0–4 DAA), Mid (7–9 DAA), and Late (14–19 DAA) stages in three biological replicates (Fig. S1a). After harvest, seeds were immediately frozen in liquid nitrogen and stored at −80 °C until processing. Lemma and palea were carefully removed to isolate caryopses, which were then ground to a fine powder in liquid nitrogen and lyophilized for downstream analyses (Fig. S1b–f).

2.2. Quantification of total starch and soluble sugars

Total starch in rice seed samples was measured using the Total Starch (AA/AMG) Assay Kit (Megazyme, Ireland). Briefly, 50 mg of lyophilized seed sample in a reaction vial was used to estimate total starch content by following manufacturer's instructions. The total starch content was calculated using the Mega-Calc™ software provided with the assay kit.

Soluble sugar content was measured using the anthrone assay as described previously (Dien et al., 2019; Verma et al., 2025). Briefly, seed tissue was finely ground using a tissue lyser, extracted with 80 % ethanol, and incubated in a water bath at 80 °C for 10 min. The extraction was repeated twice, and the supernatant was used for sugar estimation. d-Glucose was used to generate a standard curve for quantification.

2.3. Soluble phosphate (Pi), total phosphorus and phytic acid estimation

To quantify soluble Pi in seed tissue, samples were ground in liquid nitrogen and homogenized in extraction buffer (10 mM Tris-HCl, pH 8.0; 1 mM EDTA; 0.1 M NaCl; 1 mM β-mercaptoethanol) at a 1:10 ratio. The homogenate was diluted five-fold with 1 % glacial acetic acid and incubated at 42 °C for 30 min. Following centrifugation at 16,200×*g* for 10 min at 22 °C, Pi was extracted from the supernatant. A 300 μL aliquot of supernatant was then mixed with 700 μL of blue color reagent (1:6 ratio of 10 % ascorbic acid to 0.42 % ammonium molybdate in 1 N H_2SO_4), and absorbance was measured at 820 nm using a POLARstar Omega microplate reader (BMG Labtech, Germany). Pi concentration was calculated using a KH_2PO_4 standard curve, as described by Mehra et al. (2017).

Phytic acid content in rice seeds was determined using the Phytic Acid Assay Kit (Megazyme K-PHYT, Ireland) according to the manufacturer's protocol. Briefly, 50 mg of lyophilized seed sample was homogenized with 1 mL of 0.66 M HCl in a glass vial and incubated overnight at 28 °C and 180 rpm in a shaker incubator. After incubation, the samples were centrifuged at 13,000 rpm for 10 min, and 0.5 mL of the supernatant was transferred to a new tube and neutralized with 0.5 mL of 0.75 M NaOH. Subsequent steps for measuring free and total phosphorus were performed as per manufacturer's instructions. Total P and phytic acid concentration was calculated using the Mega-Calc™ software provided with the kit.

2.4. Transcriptomic analysis

Transcriptomic datasets and associated metadata from control/wild-type *Oryza sativa* seed samples were retrieved from the NCBI SRA database (Leinonen et al., 2010; Fig. S2a). Raw sequencing data in FASTQ format were downloaded using the NCBI SRA Toolkit (v3.0.0) with the prefetch and fastq-dump commands. Quality control was performed using FastQC (v0.11.7; Babraham Bioinformatics) and Fastp (Chen et al., 2018) to identify adapter sequences, remove adapters, and trim low-quality bases. After pre-processing, reads were aligned and mapped to the *Oryza sativa* Nipponbare reference genome (NCBI RefSeq)

using HISAT2 (v2.2.1; Kim et al., 2019; Table S1). Reads were then assigned to genomic features using featureCounts from the Subread package (v2.0.1; Liao et al., 2014).

2.4.1. Differential gene expression analysis

The count matrix generated by featureCounts was analyzed for differential expression using the DESeq2 package (Love et al., 2014). This analysis employed a negative binomial distribution model with a variance stabilizing transformation (VST) applied to fitted dispersion-mean relationships (Fig. S2b; Table S2). The Benjamini-Hochberg method adjusted p-values for multiple testing, with transcripts considered differentially expressed at a false discovery rate (FDR) < 0.01. Genes were considered differentially expressed when the adjusted p-value was ≤ 0.05, with an absolute fold change threshold of $-2 \leq 2$ (Fig. S2c). Principal Component Analysis (PCA) and hierarchical clustering were performed to identify the distinct sample clusters and outliers using the ggplot2 (Fig. S2d) and pheatmap (clustering heatmap; Fig. S2e) packages in R. Differentially expressed genes (DEGs) were functionally annotated using gene ontology (GO) and Kyoto Encyclopedia of Genes and Genomes (KEGG) enrichment analyses *via* the DAVID classification tool (Huang et al., 2007).

2.4.2. Co-expression network analysis

An unsigned co-expression network analysis was performed using the Weighted Correlation Network Analysis (WGCNA) package in R (Zhang and Horvath, 2005; Langfelder and Horvath, 2008). Phosphate-related genes identified through differential expression analysis served as key reference points for constructing gene networks. The normalized and variance-stabilized count matrix (VST) for the DEGs identified in the E vs. M and M vs. L comparisons was used to detect sample outliers and to identify co-expressed gene modules. A weighted adjacency matrix was constructed, where pairwise correlation coefficients determined the strength of connections between genes. This approach captures gene-gene relationships and emphasizes stronger correlations, providing a detailed understanding of gene interactions. The soft-thresholding power was set to 9, based on the approximate scale-free topology criterion, using the pickSoftThreshold function to build an unsigned network. The threshold for merging modules was set to 0.25 using the mergeCutHeight parameter. Hierarchical clustering analysis was performed to identify distinct modules of co-expressed genes, characterized by their expression patterns. Node and edge attributes for network construction were exported for modules containing guide genes associated with phosphate metabolism, transport, and reallocation (identified as DEGs), and visualized using Cytoscape 3.9.1 (Shannon et al., 2003).

2.5. Proteomic analysis

For proteomic analysis, total protein was extracted from powdered and lyophilized seed tissues from three developmental stages (Early, Mid and Late) following Chaturvedi et al. (2013). Briefly, samples were resuspended in extraction buffer [100 mM Tris-HCl (pH 8.0), 5 % SDS, 10 % glycerol, 10 mM DTT, 1 % plant protease inhibitor cocktail (Sigma P9599)], incubated 5 min at room temperature, heated at 95 °C for 2.5 min, and centrifuged. The supernatant was mixed with 1.4 M sucrose and extracted twice with TE-equilibrated phenol. Proteins were precipitated overnight at −20 °C with 0.1 M ammonium acetate in methanol, washed, air-dried, and solubilized in 6 M urea/5 % SDS. Protein concentrations were determined by bicinchoninic acid assay. For mass spectrometry, 40 μg of total protein was separated by 1D SDS-PAGE, digested with trypsin and desalted using a C18 SPE plate, as previously described (Zhang et al., 2024; Ghatak et al., 2021). Prior to mass spectrometric analysis, tryptic peptide pellets were dissolved in 4 % (v/v) acetonitrile and 0.1 % (v/v) formic acid. One microgram of purified peptides was loaded onto a C18 reverse-phase analytical column (Thermo Scientific EASY-Spray, 50 cm, 2 μm particle size). Peptide separation was achieved using a two-and-a-half-hour gradient, starting with a 4–35 % buffer B (79.9 % ACN, 0.1 % formic acid, 20 % Milli-Q water) over 90 min. Buffer A consisted of 0.1 % formic acid in Milli-Q water. The flow rate was set to 300 nL/min. Mass spectra were acquired in positive ion mode using a top-20 data-dependent acquisition (DDA) method. A full MS scan was performed at 70,000 resolution (m/z 200) with a scan range of 380–1800 m/z, followed by MS/MS scans at 17,500 resolution (m/z 200). Higher-energy collisional dissociation (HCD) was used for MS/MS fragmentation with a normalized collision energy (NCE) of 27 %. Dynamic exclusion was set to 20 s. Raw data were analyzed using the SEQUEST algorithm in Proteome Discoverer version 1.3 (Thermo, Germany) as previously described (Zhang et al., 2021; Ghatak et al., 2021). Peptides were matched against the appropriate databases plus decoys, with significant hits defined as those with high peptide confidence (FDR = 1 %) and Xcorr thresholds set at 1 per charge (2 for +2 ions, 3 for +3 ions, etc.). Variable modifications included N-terminal acetylation and methionine oxidation, with a mass tolerance of 10 ppm for parent ions and 0.8 Da for fragment ions. Up to two missed or nonspecific cleavages were permitted. No fixed modifications were applied.

Identified proteins were quantified based on total ion count and normalized using the normalized spectral abundance factor (NSAF) strategy (Paoletti et al., 2006). Differentially expressed proteins (DEPs) were identified using ANOVA followed by Tukey's HSD test to compare groups at different developmental stages (Early-Mid, Mid-Late, and Early-Late). Proteins with a p-value <0.05 were classified as DEPs.

2.6. Untargeted metabolite profiling

Metabolite profiling of lyophilized seed samples was performed using untargeted analysis *via* gas chromatography-mass spectrometry (GC-MS), following the method described by Schauer et al. (2005) with minor modifications. Approximately 20–25 mg of lyophilized seed sample was extracted with 480 μL of pure methanol, and 20 μL of a 0.2 mg mL^{-1} ribitol solution was added as an internal standard. The mixture was vigorously shaken for 2 min and then heated to 70 °C for 15 min. Following this, an equal volume of water was added, and the mixture was shaken vigorously again before the addition of 250 μL of chloroform, ensuring thorough mixing. The resulting mixture was centrifuged at 2200 g for 10 min at room temperature (~25 °C). The upper aqueous phase was carefully removed and dried in a speed vacuum rotator at 35 °C.

The dried extract was then re-dissolved in 40 μL of 20 mg mL^{-1} methoxamine hydrochloride in pyridine and incubated for 90 min at 37 °C. Afterward, 60 μL of N-methyl-N-(trimethylsilyl) trifluoroacetamide (MSTFA) was added, followed by an additional incubation for 30 min at 37 °C to facilitate derivatization. Once this process was complete, the sample was transferred to a GC-MS vial containing an insert. For the GC-MS analysis, an injection volume of 0.2 μL was utilized with a split injection mode, set at a split ratio of 5. The analysis was conducted using a Shimadzu Gas Chromatograph (GC-2010 Plus) coupled with a mass spectrometer (TQ 8050) and an autosampler (AOC-20s) with an auto-injector (AOC-20i). The separation of metabolites was achieved using an SH-Rxi-5Sil MS capillary column (30 m × 0.25 mm, 0.25 μm) from Restek Corporation, USA, with helium as the carrier gas at a flow rate of 1 mL min^{-1}. The GC method consisted of an initial isothermal heating at 80 °C for 2 min, followed by a temperature ramp of 5 °C min^{-1} to 250 °C, with a hold time of 2 min, and a final ramp of 10 °C min^{-1} with a hold time of 24 min. The total run time for the GC-MS analysis was 67 min, including a solvent delay of 4.5 min. Chromatogram integration and mass spectral analysis were performed using GC-MS solution software (Version 4.45 SP 1), and metabolite identification was carried out using the NIST14s and WILEY8 spectral libraries.

2.7. Multiomics data integration

A systems biology approach was utilized to integrate the transcriptomic, proteomic, and metabolomic datasets. Multiomics data analysis was conducted by correlating gene expression profiles (DEGs) with protein expression levels (DEPs) and metabolite concentrations, providing insights into the regulatory mechanisms driving phosphate remobilization and allocation during seed developmental processes. To capture the intricate, multi-layered interaction networks incorporating gene expression and metabolite data, we employed Weighted Gene Co-expression Network Analysis (WGCNA) in R, calculating correlations between the module eigengenes and the metabolite data using Pearson correlation. WGCNA facilitates the integration of external data, such as phenotypic traits and metabolite data, to reveal relationships between biological modules and specific traits. An eigengene represents the overall expression patterns of the module and enables efficient correlation analysis between modules and external traits (Zheng et al., 2024; Langfelder and Horvath, 2008). This analysis helped identify highly correlated module eigengenes whose expression profiles are significantly associated with the metabolite, visualized as a network using Cytoscape v3.10.2. In these networks, nodes representing differentially expressed genes (DEGs) are connected by edges that signify significant correlations or interactions derived from the metabolite data (Langfelder and Horvath, 2008; Shannon et al., 2003). This network approach allowed for identifying central nodes (hub genes or proteins) that may play pivotal roles in the regulatory network governing phosphate mobilization during rice seed development.

The integrated dataset from the transcriptome, proteome, and metabolome was further analyzed using the Plant Reactome (https://plantreactome.gramene.org), which employs the Reactome data model and enables the mapping of various rice-specific reactions and biological processes. Reactome data modeling organizes biological pathway information into a structured and interconnected format to facilitate detailed insights into molecular reactions and cellular processes. This provided detailed insights into rice-specific molecular pathways that are significantly influenced at all three biological levels: transcriptome, proteome, and metabolome (Kanehisa and Goto, 2000).

2.8. Generation of rice transgenic lines

To generate knockout lines, a single-guide RNA (gRNA) targeting the exon region of the *OsPHR3* gene was designed using the CRISPR-GE toolkit (Xie et al., 2017; http://skl.scau.edu.cn/). The gRNA was cloned into the binary vector pRGEB32 (Xie et al., 2017) and transformed into the *indica* rice genotype (IET-10364) *via Agrobacterium tumefaciens* strain EHA105, following the protocol described in Pandey et al. (2024). Transgenic plants were raised under greenhouse conditions (30 °C day/24 °C night temperatures, 16 h light/8 h dark photoperiod, 400–450 μmol photons m^{-2} s^{-1}, and ~70 % relative humidity). For mutation screening, genomic DNA encompassing the gRNA target site was amplified using PCR, cloned into the pJET 1.2 vector (Thermo Scientific), and sequenced through Sanger sequencing. Mutations were detected by comparing the sequences to the wild-type reference.

2.9. Scanning electron microscopy imaging of rice seeds

Seed morphology and starch granule packaging in wild-type (WT) and knockout (KO) seeds were visualized using a scanning electron microscope (SEM, EVO® 911 LS10 Zeiss, Germany). Mature seeds were imaged directly at 28 × magnification. To examine starch granule morphology and packaging in detail, the seeds were bisected through the center of the endosperm, and photographs were taken at 70 × and 2500 × magnifications.

2.10. Quantitative PCR analysis

Total RNA was isolated from the seed samples using TRIzol (Thermo Fisher Scientific, CA, USA). qPCR was performed as described previously (Pandey et al., 2024). The cDNA was synthesized using High-Capacity cDNA Reverse Transcription Kit (Applied Biosystems) following manufacturer's protocol. The primers used in this study were designed from the coding sequence (CDS) region of the genes using PRIMER EXPRESS version 2.0 (PE Applied Biosystems™, USA) with default parameters. qPCR was performed using the Applied Biosystems 7500 Fast Real-Time PCR system to profile gene expression. The relative expression levels of the genes were calculated using the ΔΔCt method (Livak and Schmittgen, 2001). The reactions were conducted with three biological replicates using the housekeeping gene, *Ubiquitin5* as endogenous control.

3. Results

3.1. Stage-specific partitioning of phosphate and carbon in developing rice seeds

For our study, we examined three broad stages of seed development in rice: Early (S1+S2; 2–3 DAA), Mid (S3; 7–9 DAA), and Late (S4; 17–19 DAA), each characterized by distinct morphological features and biochemical processes (Fig. S1a). During rice seed development, a coordinated shift in phosphate and carbon metabolism occurs, reflected in dynamic changes in total phosphorus (P), soluble inorganic phosphate (Pi), soluble sugars, starch, and phytic acid across developmental stages (Fig. S1b–f). There is a gradual increase in starch, phytic acid, and total phosphorus content as seed development progresses from early to late phases. However, the trend is reversed for soluble Pi and soluble sugars. This reflects a metabolic shift from early to mid to late stages, where soluble sugars and soluble Pi are mobilized for starch biosynthesis and phytic acid accumulation. Thus, our biochemical data reveal a tightly regulated, sequential process, beginning with early development characterized by phosphate supply to filial tissues to support energy requirements for growth and metabolism, followed by the mid-stage where Pi diminishes during starch synthesis; and finally, during the late stage, phosphate is gradually stored as phytic acid. This dynamic process represents the broader phosphate partitioning model observed in cereals and lays a foundation to explore the different transcriptional programs and regulatory networks that orchestrate stage-specific allocation of phosphate and carbon during rice seed development.

3.2. Temporal expression of key genes during rice seed development

We selected 43 RNA-seq datasets (among 51 curated) with an average HISAT2 alignment of 93.08 % against the *Nipponbare* reference genome for conducting transcriptomic analysis (Table S1; Fig. S2a). The variance-stabilized read count data generated using HISAT2 and featureCounts, which were used to identify differentially expressed genes, are presented in Table S2 (Fig. S2b–e). In the Early seed development versus Mid-seed filling stages (E vs. M) and Mid-seed filling stage versus Late seed maturation stage (M vs. L) comparisons, 5992 and 2980 DEGs were identified, respectively (Fig. 1a). Among the total DEGs, 1093 genes were common to both the comparisons, which accounts for 18.24 % of the E vs. M and 36.67 % of the M vs. L, showing dynamic temporal expression. This means, 81.75 % (4899 genes) were unique to the E vs. M, while 63.3 % (1887 genes) were specific M vs. L. Interestingly, during E vs. M, majority of genes were upregulated (4052 DEGs), compared to M vs. L (only 256 DEGs) (Fig. S3a).

KEGG enrichment analyses of the significantly upregulated genes during the early stage revealed enrichment in transcriptional regulation and transport-related activities, particularly those associated with photosynthesis, and the transport of nitrate, zinc, sugar and phosphate. Key phosphate-related genes that were induced during E vs. M include phosphate transporters such as *phosphate transporter PHO1-1-like*

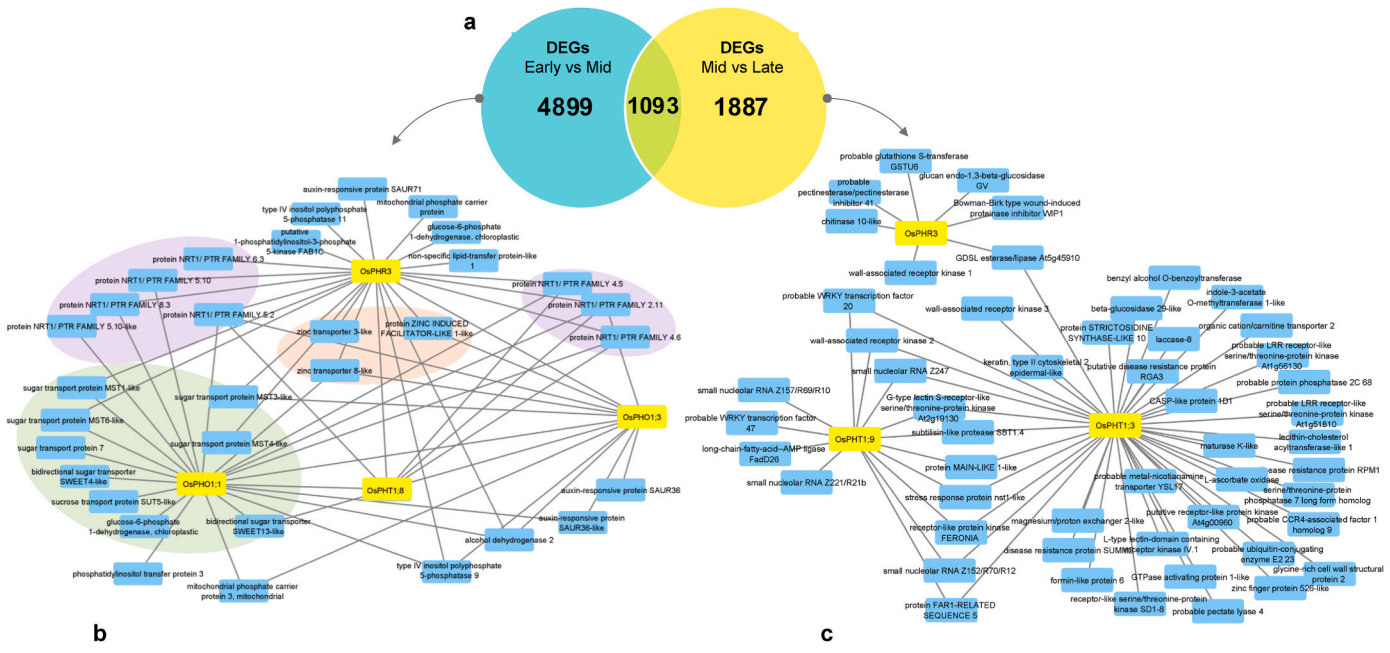

Fig. 1. Transcriptomic dynamics during rice seed development. (a) Venn diagram showing numbers of differentially expressed genes (DEGs) identified across stages: Early vs. Mid and Mid vs. Late. (b) Gene coexpression networks were constructed using DEGs from (b) E vs. M and (c) M vs. L comparisons. Hub genes *OsPHO1;3*, *OsPHO1;1*, *OsPHT1;3*, *OsPHT1;8*, *OsPHT1;9*, and *OsPHR3* (yellow nodes) are interconnected *via* various protein-coding genes, including transporters and transcription factors. Functionally related gene clusters highlighted with colored ovals indicate coordinated regulation during seed development. (For interpretation of the references to color in this figure legend, the reader is referred to the Web version of this article.)

(*OsPHO1;1 - LOC_Os01g02000*), *phosphate transporter PHO1-3-like* (*OsPHO1;3 - LOC_Os06g29790*), *inorganic phosphate transporter 1-1-like* (*OsPHT1;1 - LOC_Os03g05620.1*), *probable inorganic phosphate transporter 1–8* (*OsPHT1;8 - LOC_Os10g30790.2*), and *PHOSPHATE STARVATION RESPONSE 3-like* (*OsPHR3 - LOC_Os02g04640*) (Table S3). Whereas genes such as *phosphate transporter PHO1-2-like* (*OsPHO1;2* - LOC_Os02g56510.1), *inositol-pentakisphosphate 2-kinase IPK1-like* (*OsIPK1*; *LOC_Os04g56580.1*), *pyruvate, phosphate dikinase 1, chloroplastic-like* (*OsPPDK*; *LOC_Os05g33570.2*) were identified to be downregulated during the early stage with respect to mid stage of seed development.

During the mid to late seed developmental stages (M vs. L), the majority of DEGs (2,724) were downregulated, while only a small fraction (256) showed upregulation (Table S4). The downregulated genes included those involved in phosphate translocation, such as *OsPHT1;10* (*LOC_Os06g21950*), *OsPHT1;9* (*LOC_Os06g21920.1*), and *OsPHT1;3* (*LOC_Os10g30770.1*). Notably, *OsPHR3* was among the genes showing dynamic expression pattern, being significantly upregulated during early stages, then downregulated at the mid stage, and subsequently upregulated again during the late stage of seed development. This expression trend suggests a key regulatory role for *OsPHR3* in coordinating phosphate loading during rice seed development. Interestingly, at the mid stage, when *OsPHR3* expression declined, *OsPHO1;2* was upregulated relative to the early stage, consistent with its role in phosphate unloading from maternal cells (Ko et al., 2024). KEGG enrichment analysis further revealed that a subset of DEGs was enriched for phosphatidylinositol-4,5-bisphosphate binding, associated with various cellular signalling processes. The downregulation of these genes during the mid-seed development stage and their induced expression during late seed maturation reflect a broader shift in molecular processes as seed development progresses towards maturation.

The expression of ten differentially expressed phosphate-related genes identified from the E vs. M and M vs. L comparisons was analyzed across the 43 datasets representing developmental stages, S1 to S4 (Table S2; Fig. S3b). Notably, genes such as *OsPHR3*, *OsPHO1;1*, and *OsPHT1;1* showed higher expression during the early stages, whereas there is an evident decline in the expression levels of these genes, during the mid-developmental stages. However, during the late maturation stage, the expression of most phosphate-related genes slightly increases, with the exception of *PHOSPHATE STARVATION RESPONSE 1-like* (*PHR1-like: LOC_Os03g21240.1*), which remains consistently expressed throughout the developmental stages. The hierarchical clustering of all the DEGs based on their expression reveals a close association of *OsPHR3* with genes encoding NRT1/PTR FAMILY 8.3 protein, NRT1/PTR FAMILY 2.11 protein, sugar transport protein MST1, zinc transport 8, with very similar expression patterns (Fig. S3c). This suggests that these nitrate, sugar and zinc transporters are co-expressed with *OsPHR3* and may be coordinately regulated for their transport activities. This relationship, along with several others will be further investigated using gene co-expression network (GCN) analysis.

3.3. Gene co-expression network reveals sophisticated phosphate regulatory system

To understand the relationships among the co-expressed genes, a weighted gene co-expression network was generated, where nodes represent DEGs, edges represent the weighted co-expression relationships. The hub genes are those with the highest connectivity, that may play key regulatory roles within co-expressed gene modules, providing insight into the structure and function of complex biological networks.

3.3.1. Gene co-expression network of DEGs from early-vs mid-developmental stages

The sample clustering analysis of 5992 DEGs identified during E vs. M, revealed no outliers among the 43 samples, indicating a homogeneous dataset suitable for subsequent analyses (Fig. S4a–b; Table S5). Gene co-expression network (GCN) analysis revealed nine distinct modules, with the largest 'turquoise' module comprising 3547 genes (Fig. S4c). Since a significant proportion of phosphate-related genes were identified within this module, the corresponding DEG-Network was visualized to identify and study the 'hub' genes associated with phosphate metabolism. To explore the relationships between co-

expressed genes related to phosphate metabolism, we focused on the selected phosphate metabolism-related genes connecting to other co-expressed genes with higher weight attributes, excluding uncharacterized, housekeeping, and redundant genes. However, the complete network file containing the edge list, where each row represents a pair of co-expressed genes (nodes) with their weight or score for the connection (edge), has been provided in Table S6. This analysis identified four key hub genes, namely *OsPHR3*, *OsPHO1;1, OsPHO1;3*, and *OsPHT1;8,* which interconnect *via* various protein-coding genes, including transporters and transcription factors, and are likely to play crucial roles in regulating phosphate homeostasis (Fig. 1b).

Several important genes encoding NRT1/PTR FAMILY proteins (such as NRT1/PTR FAMILY 4.6, 8.3, and 5.10) were identified. Notably, NRT1/PTR FAMILY 4.6 connects three of the hub genes (*OsPHR3*, *OsPHO1;1,* and *OsPHT1;8*), while NRT1/PTR FAMILY 4.5, 2.11, and 5.2 are connected to all four hub genes. These genes, primarily functioning as nitrate transporters, showed significant downregulation in the M vs. L comparison, suggesting that their transporter activity is regulated during the early phases of seed growth. Additionally, in the same GCN, co-expressed genes encoding zinc transporters such as zinc transporter 3, ZINC INDUCED FACILITATOR, zinc transporter 8 were connected to *OsPHR3*, *OsPHO1;1* and *OsPHO1;3*, indicating a possible phosphate-zinc crosstalk mediated by *OsPHR3*.

Furthermore, the DEG-Network highlights the critical role of sugar transporter genes during the early seed development. Genes encoding *sugar transport protein MST1* connects *OsPHR3* and *OsPHO1;1*, while *sugar transport protein MST3* is co-expressed with *OsPHR3* and *OsPHO1;3*. *Sugar transport protein 7, bidirectional sugar transporter SWEET4-like* and *sucrose transport protein SUT5-like* are associated with *OsPHO1;1*. Additionally, the *bidirectional sugar transporter SWEET13-like,* connects both *OsPHO1;1* and *OsPHT1;8* (Fig. 1b). All these sugar transporter genes are significantly upregulated during the early stage while downregulated during the mid-developmental phase. Their co-expression with Pi transporters suggests an integrated regulatory mechanism coordinating Pi and carbon metabolism. This coordination, particularly between sucrose and Pi transport indicates a potential role for phosphate metabolism in regulating sugar transport, possibly for nutrient partitioning.

3.3.2. Gene co-expression network of DEGs from mid versus late developmental stages

The GCN analysis conducted on 2980 DEGs from the M vs. L comparison resulted in eight co-expressed gene modules, including the biggest modules, the 'turquoise,' 'blue,' and 'brown', comprising 726, 283, and 174 genes, respectively (Fig. S4d). This DEG-Network is centered around three hub genes associated with phosphate metabolism, *OsPHR3, OsPHT1;3* and *OsPHT1;9*, interconnected *via* several receptor protein-encoding genes. *OsPHT1;3* is connected to *OsPHR3 via GDSL esterase/lipase At5g45910*, and to *OsPHT1;9* through *wall-associated receptor kinases 2* (*WAK2)*. The association of WAKs with *OsPHR3* and *OsPHT1;9* suggests their potential involvement in cellular signaling (Chen et al., 2021; Zhang et al., 2023). The GCN also reveals a strong co-expression of *OsPHR3* with several genes involved in stress response, cell wall modification and signaling, including *GSTU6*, *glucan endo-1, 3-beta-glucosidase*, *Bowman-Birk type wound-induced proteinase inhibitor*, *pectinesterase/pectinesterase inhibitor 41, chitinase 10 and WAK1*. This network cluster suggests that *OsPHR3* might also modulate stress signaling, particularly during late seed development. (Fig. 1c; Table S7; S8). All these genes are downregulated during the mid-stage compared to the late developmental stages, indicating their predominant role in the latter phase.

3.4. Stage-specific and core protein expression patterns during seed development

Our proteomic analysis detected 3230 proteins in the rice caryopsis across three developmental stages, namely, early (E), mid (M), and late (L) stage (Table S9; Fig. S5a). Principal component analysis (PCA) revealed distinct grouping into clusters underscoring the similarity in protein expression profiles within each cluster, representing E (red), M (blue), and L (green) (Fig. 2a). The PCA showed clear separation of E and M samples from L samples by the first principal component PC1, which accounted for 78.65 % of the variance. Of the 3230 proteins identified, 2020 (62.5 %) were consistently expressed across all developmental stages, while 158 (4.9 %) were unique to the Early stage, 48 (1.5 %) to the Mid-stage, and 65 (2 %) to the Late stage, representing stage-specific proteomes. This distribution is illustrated using a Venn diagram (Fig. 2b). Functional annotation and GO term analysis assigned the commonly expressed proteins to essential core components, involved in functional processes like energy production, cellular signalling, cell division, and stress response. The uniquely expressed proteins in the early stage (158 proteins) were primarily involved in cell division and early growth, including metabolic enzymes, regulatory proteins, proteins associated with stress-response, structural components, DNA repair and replication. Mid-stage-specific proteins (48) were primarily associated with spatial organization of seed tissues (e.g., pattern formation proteins, no apical meristem proteins), signalling pathways (calcium/calmodulin-dependent kinases), and nutrient storage (e.g., LTPL83 and seed storage proteins).

Interestingly, the global proteomic data identified several proteins/enzymes directly involved in phosphate metabolism, including inositol monophosphatase 3 (*LOC_Os03g39000.2*), *myo*-inositol-1-phosphate synthase (*LOC_Os03g09250.1*), inositol-tetrakisphosphate 1-kinase 6-like (*LOC_Os09g34300*), dolichol-phosphate mannosyltransferase subunit 1 (*LOC_Os03g60939*) and phosphate carrier proteins (*LOC_Os02g52860.1*; *LOC_Os06g10810.1*). These enzymes are key components of the inositol phosphate metabolic process and phosphatidylinositol phosphate biosynthetic pathway, which are crucial for the synthesis of PA (inositol hexakisphosphate, IP6), the primary storage form of phosphorus in seeds (Raboy, 2003, 2009).

3.5. Differentially expressed proteins involved during seed development

Out of the 3230 proteins identified through proteomic profiling, 753 (Table S10), 1036 (Table S11), and 1516 (Table S12) differentially expressed proteins (DEPs) were found in Early vs. Middle (E vs. M), Middle vs. Late (M vs. L), and Early vs. Late (E vs. L) comparisons, respectively (Fig. 2c). This study primarily focuses on DEPs from the E vs. M and M vs. L comparisons, as these capture critical transitions from early differentiation (E) to nutrient accumulation, and from storage (M) to maturation (L) during seed development (Fig. S5a). In E vs. M, DEPs were significantly enriched for the GO term GO:0009507 (chloroplast), with 186 proteins involved in metabolic processes, followed by 132 proteins in secondary metabolite biosynthesis and 96 proteins in ATP binding. Key DEPs associated with phosphate metabolism include inositol-3-phosphate synthase 1 (*OsMIPS1*; *LOC_Os03g09250.1*) and probable phosphoinositide phosphatase SAC9 (*LOC_Os01g25330.1*). In M vs. L, nutrient reservoir activity (GO:0045735) exhibited the highest enrichment score (11.57), linked to starch biosynthesis processes and proteins such as starch synthase 3 (*OsSSIII*; LOC_*Os08g09230.2*) and sucrose-phosphate synthase 4 (*LOC_Os08g20660.1*). Additionally, 223 proteins were involved in metabolic processes, including inositol-pentakisphosphate 2-kinase IPK1-like (*OsIPK1*; *LOC_Os04g56580.1*), and inositol-tetrakisphosphate 1-kinase 6-like (*LOC_Os09g34300*), which play critical roles in phosphate metabolism during the transition from the mid to late stages of seed development. Proteins/enzymes including MIPS1, IPK1, and SSIII showed elevated expression during the mid-to-late stages, whereas glucose-6-phosphate/phosphate translocator 2 (*OsGPT2*; LOC_Os07g33910.2) exhibited higher protein abundance during the early-to-mid developmental stages (Fig. 2d).

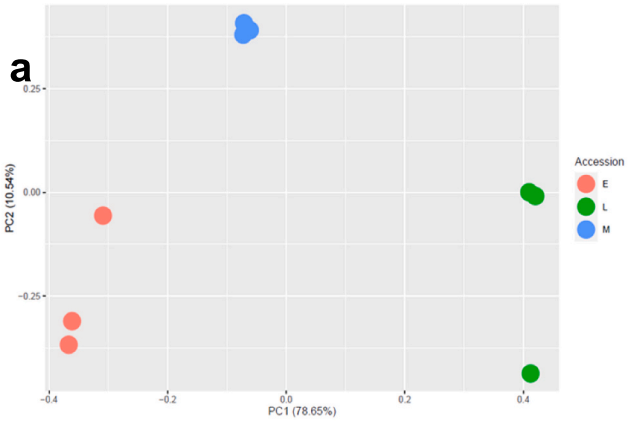

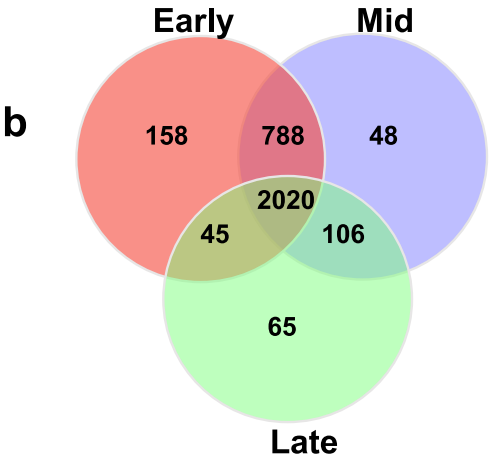

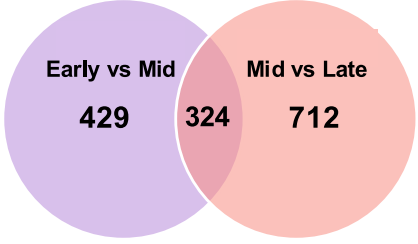

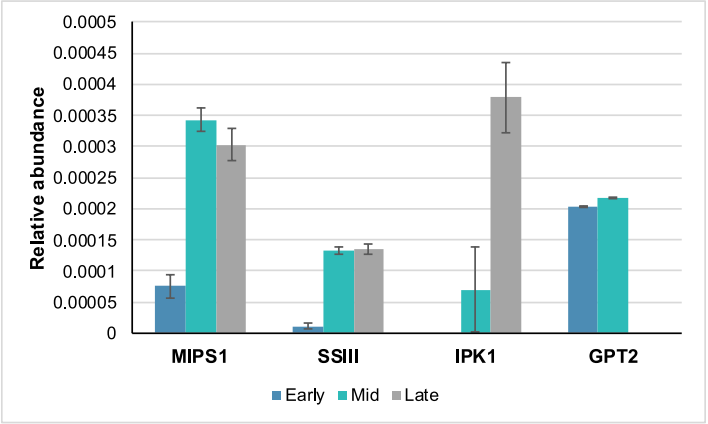

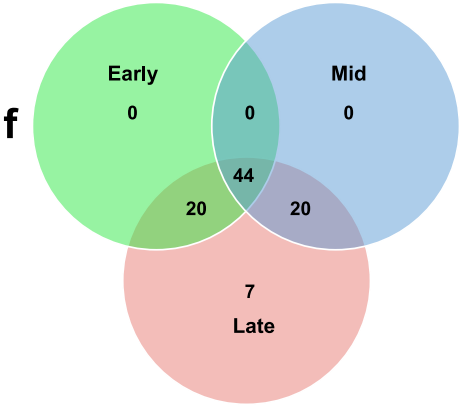

(caption on next page)

Fig. 2. Proteomic and metabolomic overview across Early, Mid, and Late stages of rice seed development. (a) Principal component analysis (PCA) of seed samples representing early (E-red), mid (M-blue) and late (L-green) stages. (b–c) Venn diagram showing the number of: (b) proteins identified as stage specific and core proteins, and (c) differentially expressed proteins (DEPs) identified in E vs. M and M vs. L comparisons. (d) Bar graph showing the relative abundance (normalized spectral abundance factor, NSAF) of selected DEPs across the early-to-late transition stages. Data are presented as mean ± SE (n = 3). (e) Heatmap showing the normalized metabolite levels (log transformed values; n = 3) of 91 differentially accumulated metabolites (DAMs) across early, mid, and late seed developmental stages. The color scale represents normalized stage-specific metabolite levels, with red indicating relatively high abundance and blue indicating relatively low abundance. (f) Venn diagram illustrating the unique and shared differentially accumulated metabolites (DAMs) identified across the E, M, and L stages. (For interpretation of the references to color in this figure legend, the reader is referred to the Web version of this article.)

3.6. Differentially accumulated metabolites during seed development

Metabolite profiling during seed development was performed using GC-MS, resulting in the identification of 91 differentially accumulated metabolites (DAMs) across early, mid, and late developmental stages (Table S13; Fig. S5b). During the early and mid-developmental stages, 42 metabolites were detected in each stage, while seven in the late stage. To elucidate the temporal dynamics of these metabolites during seed development, unsupervised hierarchical clustering was conducted (Fig. 2e). The heatmap reveals stage-specific accumulation patterns of 91 metabolites across early, mid, and late developmental phases. Among these DAMs, 44 were shared across all stages and 7 were exclusive to the late stage (Fig. 2f). A subset of metabolites, including phosphorylated sugars such as glucose-6-phosphate and *myo*-inositol 1,3,4,5,6-pentakisphosphate, showed marked enrichment at the mid stage, indicating heightened metabolic activity associated with phytic acid biosynthesis. Notably, key metabolites such as alanine, glucose-6-phosphate and *myo*-inositol 1,3,4,5,6-pentakisphosphate followed a distinct temporal trajectory peaking at the mid stage and declining thereafter, suggesting their transient role in nutrient storage and energy metabolism during seed filling. The accumulation of these metabolites including glucose-6-phosphate and in the mid seed filling stage aligns well with the transcriptomic and proteomic data.

3.7. Transcriptomic and proteomic analysis unveils carbon and phosphate regulation

A total of 7879 DEGs were compared with 1400 DEPs, which included data from both the E vs. M and M vs. L comparisons to identify common entities. We identified 297 entities common to both datasets, reinforcing the role of this subset of genes/proteins during seed development (Table S14; Fig. 3a). These genes/proteins were predominantly involved in metabolic processes, such as starch and sucrose metabolism (beta-fructofuranosidase 1; *LOC_Os04g45290.1*, beta-glucosidase BoGH3B; *LOC_Os03g53800.5*, starch synthase 3; (*OsSSIII) LOC_Os08g09230.2*, sucrose-phosphatase 2-like; *LOC_Os02g05030.1*), lipid biosynthesis (acyl-[acyl-carrier-protein] desaturase 4; *LOC_Os03g30950.1*, allene oxide synthase 1; *LOC_Os03g09250.1*, phospholipase A1-II 5-like; *LOC_Os01g51360*), and phenylpropanoid biosynthesis (aldehyde dehydrogenase family 2 member C4; *LOC_Os01g40860*, peroxidase 35; *LOC_Os03g55420*, peroxidase P7; *LOC_Os01g10850*, probable caffeoyl-CoA O-methyltransferase; *LOC_Os09g30360*).

During the early to mid-developmental phases (E vs. M), 68 genes/proteins were identified, whereas only 11 genes/proteins were detected during the mid to late phases (M vs. L), (Fig. 3b). Notably, genes, namely, *OsMIPS1*, *OsIPK1, OsSSIII* and *OsGPT2* exhibited induced expression during the mid seed filling stage in both transcriptomic and proteomic datasets. These genes are primarily associated with phytic acid and starch biosynthesis.

3.8. Transcriptomic and metabolomic analysis reveals phytic acid regulatory network

To integrate transcriptomic data with identified metabolites from seed samples representing three developmental phases, we conducted co-expression network analysis using WGCNA. Our study focused on examining the role of genes, proteins, and metabolites associated with phosphate metabolism during seed development in *Oryza sativa*, placing particular emphasis on the metabolite *myo*-inositol 1,3,4,5,6-pentakisphosphate (hereafter referred to as '*myo*'). We incorporated our metabolite data into WGCNA to identify module eigengenes that are highly correlated with '*myo*', revealing gene networks responsive to this variable. In our analysis, two module eigengenes, MEgreenyellow and MEmagenta, were found to be tightly correlated with '*myo*' (Fig. 3c-d). The node-to-node attributes of these modules were then exported and visualized as a DEG-myo-Network (Table S15). We identified three major hub genes, *OsMIPS1*, *putative lipid phosphate phosphatase 3, chloroplastic* (*LOC_Os01g04660*), and *phosphatidylinositol 4-kinase gamma 4* (*PI4Kγ4; LOC_Os01g13360.1*). *OsMIPS1* and *putative lipid phosphate phosphatase 3* were directly connected, while *OsMIPS1* and *phosphatidylinositol 4-kinase gamma 4* were linked *via inositol-tetrakisphosphate 1-kinase 4-like* (*LOC_Os02g26720*). Notably, *PI4Kγ4* was also directly connected to *starch synthase 3* and *phosphate transporter OsPHO1;2*, which were interconnected. Interestingly, *PI4Kγ4* also showed connections with *glycerophosphodiester phosphodiesterase GDPD1, chloroplastic* (*LOC_Os02g31030.1*) and *purple acid phosphatase 3* (*LOC_Os10g02750*) (Fig. 3e). For clarity and to focus on phosphate metabolism-associated genes, we excluded uncharacterized genes and those with housekeeping roles, such as those involved in translation and general developmental processes.

3.9. Multiomics data highlights the critical role of OsMIPS1

The genes identified from module eigengenes by integrating transcriptomic and metabolite data were compared with identified DEPs to detect 126 common genes. GO and KEGG enrichment analyses identified that these 126 genes were predominantly associated with metabolic pathways, biosynthesis of secondary metabolites, and nutrient reserve activity (Fig. 4a; Table S16). The DEG-myo-DEP-Network generated from this subset identified four hub genes, including *OsMIPS1*, *OsSSIII*, *pyruvate phosphate dikinase 1* (*OsPPDK1*) and *protein phosphatase 2C 27*. *OsMIPS1* is found connected to *OsSSIII via alanine aminotransferase 2 (OsAlaAT2) and pyruvate phosphate dikinase 1 (OsPPDK1)*. Pathway enrichment analysis further highlighted their involvement in metabolism and regulation, emphasizing phytic acid and *myo*-inositol biosynthetic pathways involving *OsMIPS1* (Fig. 4b; Kuwano et al., 2009). Among the 126 genes, 68 exhibited gene coexpression and connections with *OsMIPS1*, including various seed storage and stress tolerance-associated genes (vicilin-like seed storage proteins, oleosins, late embryogenesis abundant proteins, AP2-like ethylene-responsive factors, homeobox proteins, chaperones, universal stress proteins, and aquaporins, ABA-inducible proteins), all of which showed a direct connection to *OsMIPS1* (Fig. 4c; Table S17). This clearly suggests their coordinated role in the storage of energy (lipids) and phosphorus (phytate), as well as in development and environmental response in developing rice seeds.

3.10. Functional validation of OsPHR3 reveals key role during seed development

Insights gained from the multiomics analysis validated the role of *OsPHR3* in seed development by generating knockout mutant lines in rice using CRISPR/Cas9 technology. Two mutant lines, *osphr3_ko1* and

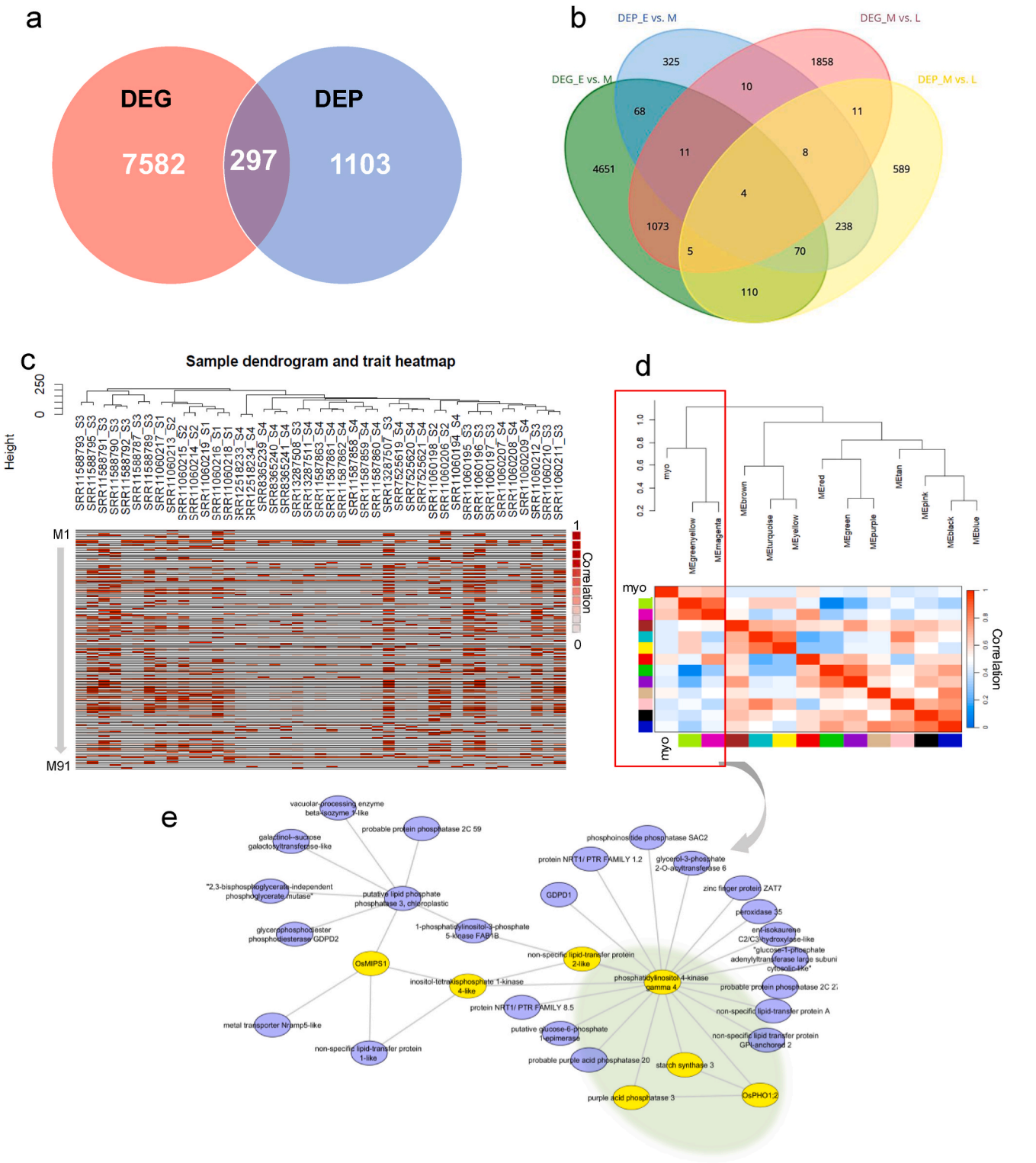

Fig. 3. Multiomics data integration reveals key metabolites and gene modules across seed developmental stages. (a) Venn diagram showing the number of differentially expressed genes (DEGs) identified *via* transcriptomics and differentially expressed proteins (DEPs) detected *via* proteomics in the early vs. mid comparison (E vs. M), and mid vs. late (M vs. L) stage comparisons. (b) A four-way Venn diagram illustrating the overlap among DEGs and DEPs across the E vs. M and M vs. L comparisons. (c) Sample dendrogram and trait heatmap showing correlations between the relative abundance of 91 metabolites (M1-M91) and 43 transcriptome samples. Positive correlations are indicated by increasing red color intensity. (d) Heatmap displaying correlations between module eigengenes and the metabolite, *myo*-inositol 1,3,4,5,6-pentakisphosphate (abbreviated as '*myo*'). The color scale represents correlation strength, with red indicating strong positive correlations and blue strong negative correlations. (e) Co-expression network of '*myo*'-associated modules derived from the MEgreenyellow and MEmagenta modules, illustrating interactions among DEGs significantly correlated with 'myo'. Nodes represent individual DEGs, while edges denote statistically significant correlations or functional associations. (For interpretation of the references to color in this figure legend, the reader is referred to the Web version of this article.)

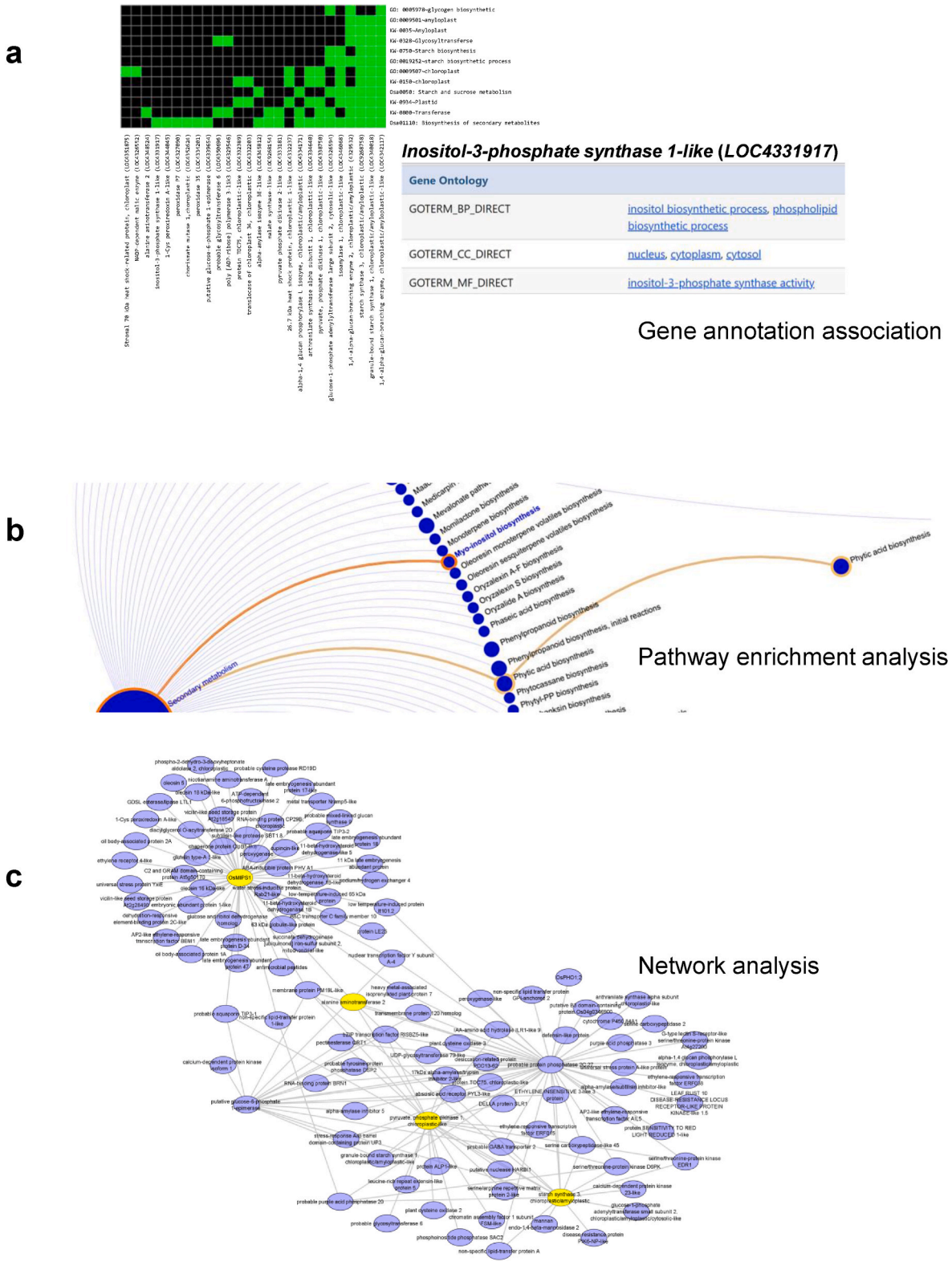

Fig. 4. Multiomics data integration reveals the key role of *OsMIPS1* in phytic acid biosynthesis. A set of 126 genes differentially expressed at both transcriptomic and proteomic levels, with strong positive correlation to *myo*-inositol 1,3,4,5,6-pentakisphosphate accumulation, were subjected to functional enrichment analysis using DAVID (https://davidbioinformatics.nih.gov/tools.jsp). (a) Functional annotation clustering highlights *inositol-3-phosphate synthase 1* (*OsMIPS1*) associations with other genes (bottom) and with Gene Ontology (GO) terms (right); green indicates similar annotations, whereas black indicates little or no association. (b) Pathway enrichment analysis confirms the role of *OsMIPS1* in *myo*-inositol biosynthesis and lipid-independent phytic acid biosynthetic processes. (c) Network of the 126 genes, with key gene highlighted in yellow. (For interpretation of the references to color in this figure legend, the reader is referred to the Web version of this article.)

osphr3_ko2, were selected based on sequencing confirmation of targeted mutations (Fig. 5a–d). Phenotypic analysis comparing these knockout lines to wild-type (WT) revealed that while seed germination rates remained comparable , key seed quality parameters, including panicle length , seed length , seed width and 100-seed weight were significantly reduced in the *osphr3* mutants (Fig. 5e-l).

To further investigate grain filling and seed quality, we assessed the morphology and packaging of starch granules using scanning electron microscopy (SEM). SEM imaging showed that starch granules in mutant seeds were unevenly packaged with undefined edges, whereas WT seeds exhibited characteristic polyhedral-shaped starch granules (Fig. 6a). Concurrently, starch content was significantly reduced in the mutant seeds compared to WT (Fig. 6b). These results demonstrate that both the quantity and quality of starch were impaired in the *osphr3* knockout lines. In addition to reduced starch content, we observed a significant decline in total seed P and phytic acid content in the mutant lines relative to WT (Fig. 6c–d). Furthermore, the *osphr3* knockout led to altered expression of genes involved in starch and phytic acid biosynthesis, namely, *OsMIPS1*, *OsIPK1*, *OsGPT2*, *OsSSIII*, along with the phosphate transporter genes *OsPHO1;1, OsPHO1;2, OsPHO1;3, OsPHT1;1* (Fig. 7a–i).

3.11. Quantitative PCR validation of key phosphate-related genes

We validated the expression of 12 phosphate-related genes identified from multiomics analysis across early, mid, and late developmental stages using quantitative PCR (qPCR). These included phosphate transporters (*OsPHT1;1, OsPHT1;3, OsPHT1;8,* and *OsPHT1;9*), *OsPHO1* homologues (*OsPHO1;1, OsPHO1;2,* and *OsPHO1;3*), a transcription factor (*OsPHR3*), regulators of starch (*OsGPT2*, *OsSSIII*) and phytic acid biosynthetic genes (*OsMIPS1* and *OsIPK1*). The details of the primer sequences used for qPCR validation are listed in Table S18. Notably, the expression of phosphate transporter genes declined during the mid-developmental stage but was relatively higher at the early stage. In contrast, genes such as *OsGPT2*, *OsSSIII, OsMIPS1* and *OsIPK1*, showed an increasing expression trend from early to late stages (Fig. S6a–l).

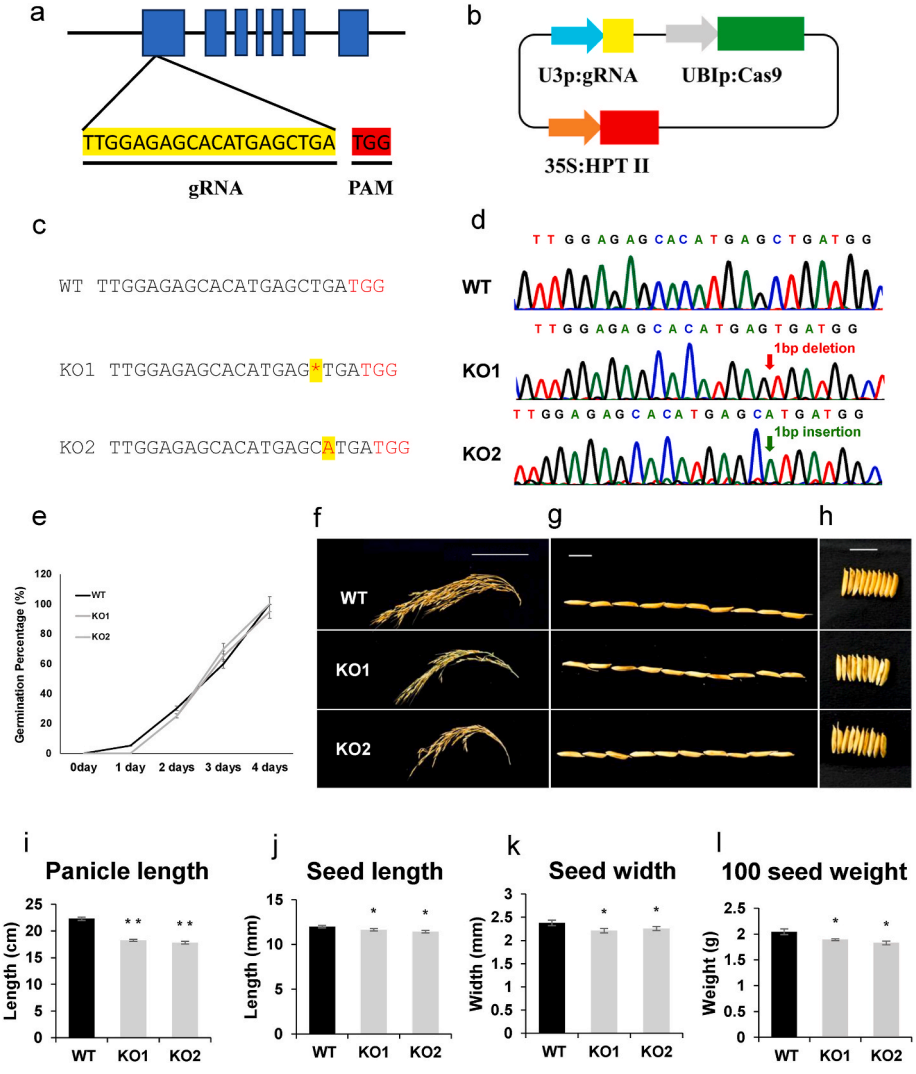

Fig. 5. Generation of *osphr3* mutant lines and phenotypic characterization of mature seeds compared with wild-type. a) Schematic representation of the *OsPHR3* gene structure showing gRNA target site. Exons are shown as blue boxes; introns as line; the PAM motif is shown in red and the gRNA sequence is highlighted in yellow. b) Map of pRGEB32 vector used to generate knock-out lines. c) Sequencing result of the *osphr3* mutant lines. d) Representative chromatogram of the sequencing for WT and *osphr3* mutant lines. (e) Germination percentage of wild-type (WT), *Osphr3-ko1* (KO1), and *osphr3-ko2* (KO2) over four days. (f) Comparative images of panicles from WT, KO1, and KO2 (Scale bar: 10 cm). (g) Seed length phenotype (scale bar: 1 cm). (h) Seed width phenotype (scale bar: 1 cm). (i) Panicle length (in cm), (j) seed length (in mm), (k) seed width (in mm), (l) 100-seed weight (in g) in WT, KO1, and KO2 (n = 30). Data are presented as means ± SE (n = 4). Statistical significance was determined using Student's t-test: P ≤ 0.05, **P ≤ 0.01, ***P ≤ 0.001, indicating significant difference from the WT control. (For interpretation of the references to color in this figure legend, the reader is referred to the Web version of this article.)

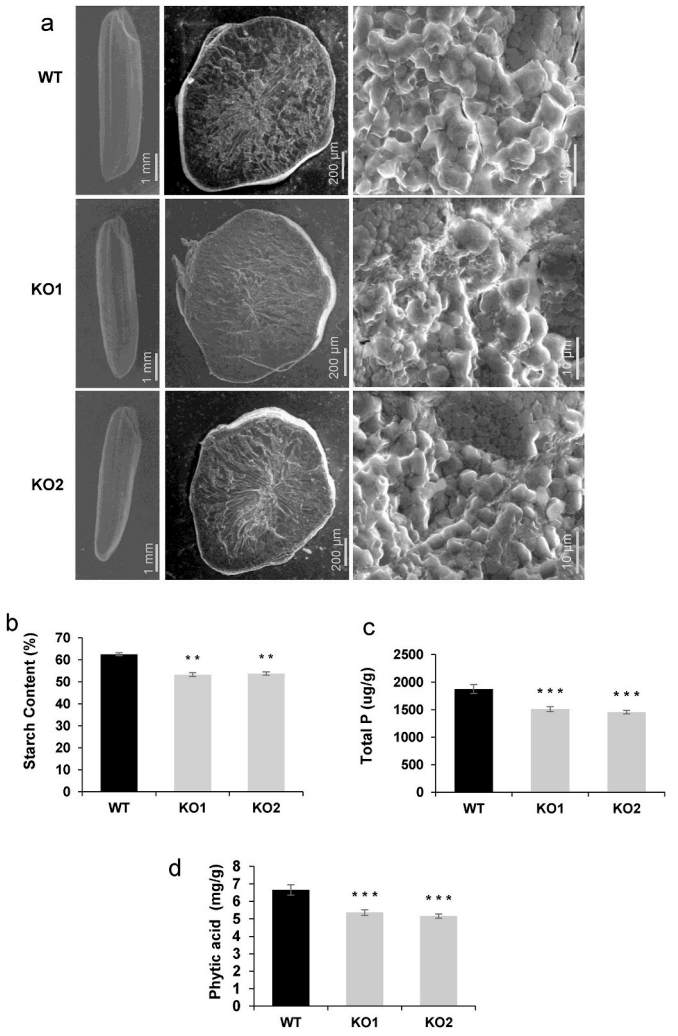

Fig. 6. Biochemical characterization of mature seeds of *osphr3* knockout compared to wild-type. (a) Scanning electron microscopy (SEM) images of seeds showing starch granules (scale bars: 1 mm, 200 μm, and 10 μm). (b) Starch content. (c) Total phosphorus (P) content. (d) Phytic acid content. Data are presented as means ± SE (n = 4). Statistical significance was determined using Student's t-test: P ≤ 0.05, **P ≤ 0.01, ***P ≤ 0.001, indicating a significant difference from control (WT).

These qPCR results were consistent with our transcriptomic data and aligned well with biochemical measurements of starch, phytic acid, and total phosphate content.

4. Discussion

Seed development, particularly endosperm formation and grain filling, largely determine crop yield. Inorganic phosphate (Pi) forms a critical nutrient, with 60–85 % Pi translocate to seeds, where a majority (65–85 %) ultimately accumulates as phytic acid (Che et al., 2020; Raboy, 2001, 2009). Although the primary Pi storage form, phytic acid reduces bioavailability of essential minerals (Fe, Zn, Ca) in human diets by forming insoluble complexes. The process of nutrient translocation, particularly of Pi, is critically regulated by several Pi transporters, especially those in the PHT and PHO families, which play key roles during seed development. Several attempts have aimed to reduce phytic acid levels by targeting *myo*-inositol derivatives and related biosynthetic pathway genes, including *myo-inositol 1-phosphate synthase*, *inositol monophosphatase*, *myo-inositol oxygenase*, and *myo-inositol O-methyltransferase,* with highly variable success and often negative pleiotropic effects on grain weight and seed viability in different crops (Alok et al., 2022; Aggarwal et al., 2018; Ali et al., 2013; Dong et al., 2013; Li et al., 2014). Similarly, enhancing phosphate use efficiency (PUE) by overexpressing Pi transporter genes has frequently resulted in Pi toxicity and stunted plant growth (Gu et al., 2016; He et al., 2019; Wang et al., 2018, 2021). These findings underscore that manipulating individual genes is unlikely to achieve sustainable improvements in PUE and yield, a systems-level approach is necessary to reconcile yield, PUE, and nutritional quality in future rice varieties. Therefore, to unravel the intricate Pi dynamics and understand the molecular mechanisms integrating Pi transport, carbohydrate metabolism, and PA biosynthesis during seed development, we employed a comprehensive multiomics approach. This approach allows us to investigate the process at multiple molecular levels and identify key regulatory players. By integrating transcriptomic, proteomic, and metabolomic data, we aimed to understand the complex interplay between Pi transport, carbohydrate metabolism, and phytic acid accumulation. This understanding, coupled with functional and expression validation of key regulators and Pi transporters, facilitates the development of rice varieties with improved PUE and reduced phytic acid content, ultimately contributing to sustainable agriculture and enhanced nutritional value.

4.1. Phosphate transport dynamics during early to late developmental transitions

Seed development in rice is clearly defined and categorized into five distinct stages. It begins post-fertilization with stage 1 (S1; 0–2 DAA), followed by stage 2 (S2; 3–4 DAA), stage 3 (S3; 5–10 DAA) corresponds to the milky endosperm stage, stage 4 (S4; 11–20 DAA) is marked by hard dough stage, and finally, stage 5 (S5; 21+ DAA) involves seed desiccation and dormancy (Agarwal et al., 2011). For transcriptome analysis, RNA-seq datasets from S1 to S4 were consolidated into three developmental phases: Early (S1 + S2), Mid (S3), and Late (S4). Differential expression profiling revealed distinct temporal patterns among phosphate transporter genes. Genes, *OsPHO1;1*, *OsPHO1;3* and *OsPHT1;1* were significantly upregulated during the early phase, consistent with roles in phosphate loading into developing seeds. In contrast, *OsPHO1;2* expression was specifically induced during the mid seed-filling stage, aligning with its reported function in unloading phosphate from maternal tissues. While *OsPHO1;1* reloads Pi into the phloem of diffuse vascular bundles (DVBs) for distribution to developing seeds, *OsPHO1;2* plays a crucial role in Pi efflux from maternal tissues during grain filling mid developmental stage in rice (Che et al., 2020; Ko et al., 2024; Wang et al., 2021). These findings indicate a stage-dependent partitioning of function among Pi transporters, with early stages dedicated to active phosphate acquisition and loading, and mid stages facilitating nutrient storage. A general decline in Pi transporter expression from early to mid-development was observed, suggesting a developmental shift from nutrient uptake and translocation toward reserve accumulation, predominantly starch during grain filling. Moreover, the relatively small overlap (~12 %) in differentially expressed genes (DEGs) between Early vs. Mid and Mid vs. Late comparisons underscores the high degree of stage specificity in transcriptional regulation, reflecting the distinct physiological priorities and developmental programs operating at each transition.

4.2. Network-based insights into phosphate-carbon-stress crosstalk

A DEG-myo-Network was constructed from module eigengenes exhibiting strong correlation with *myo*-inositol 1,3,4,5,6-pentakisphosphate (myo), identified as a differentially accumulated metabolite. In this network, nodes represent DEGs connected by edges that signify significant correlations. In this network, the phosphate transporter *OsPHO1;2* formed connections with *OsSSIII*, *phosphatidylinositol 4-kinase gamma 4* (*PI4Kγ4*), and *purple acid phosphatase 3* (*PAP3*, *LOC_Os03g13540*) within a regulatory module (Fig. 3e; Fig. 4c;

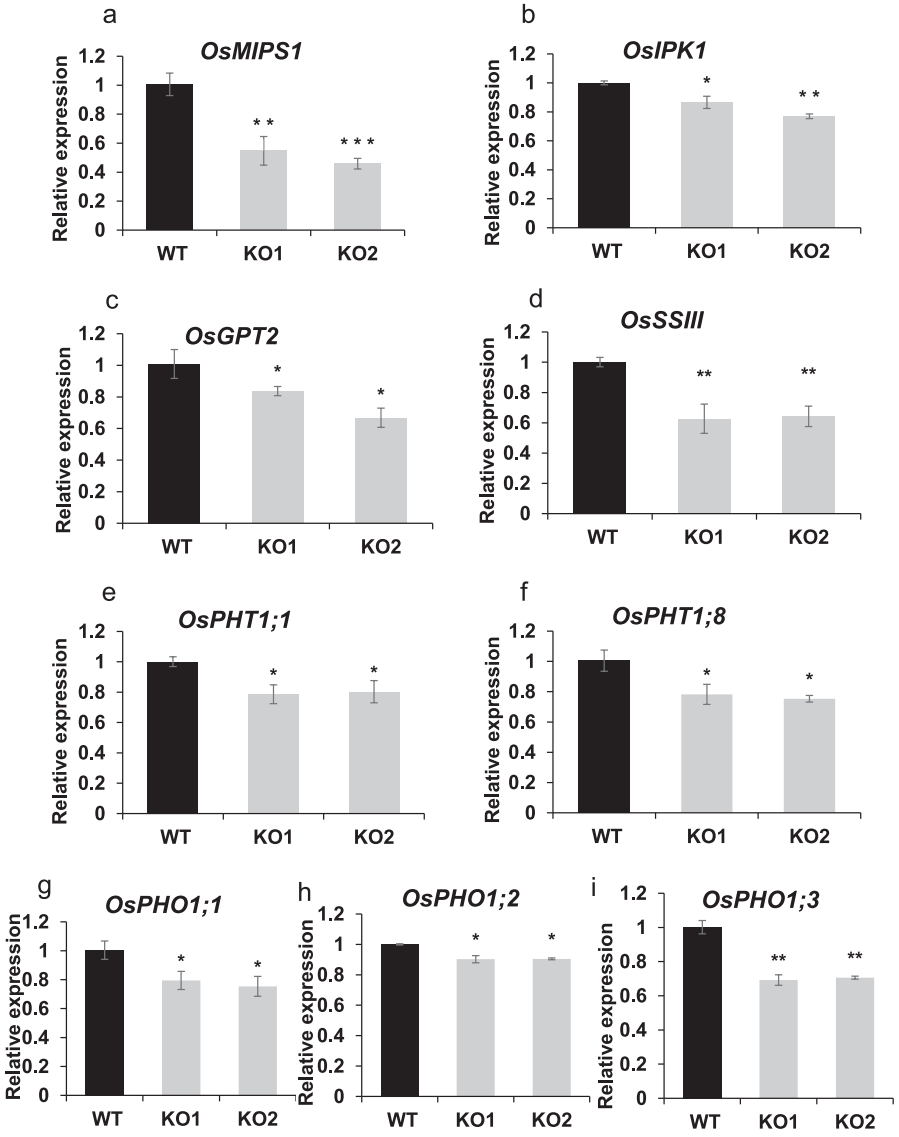

Fig. 7. Altered expression of key genes of phytic acid metabolic pathway, starch metabolism and phosphate homeostasis in the seeds of *osphr3* knockout lines. Relative expression of (a) *OsMIPS1*, (b) *OsIPK1*, (c) *OsGPT2*, (d) *OsSSIII*, (e) *OsPHT1;1*, (f) *OsPHT1;8*, (g) *OsPHO1;1*, (h) *OsPHO1;2*, and (i) *OsPHO1;3* genes in the seeds of CRISPR/Cas9-mediated *osphr3_ko1* (KO1) and *osphr3_ko2* (KO2) lines, compared to wild-type (WT). Data are presented as means ± SE (n = 3). Statistical significance was determined using Student's t-test: P ≤ 0.05, **P ≤ 0.01, ***P ≤ 0.001.

Table S15). In rice, *SSIIIa* is essential for normal polyhedral seed starch granule formation, with loss-of-function mutants exhibiting white-core, floury endosperm phenotypes (Toyosawa et al., 2016; Ryoo et al., 2007). The *PI4Kγ4* protein is primarily implicated in stress response signaling pathways (Delage et al., 2012), though its specific roles during seed development remain poorly characterized. Purple acid phosphatases (PAPs) regulate phytate metabolism and phosphate homeostasis during seed maturation, with *OsPAP3* being highly expressed in rice endosperm (Bhadouria et al., 2023; Mehra et al., 2017; RicexPro Database). This network therefore integrates core pathways of starch biosynthesis (*OsSSIII*), phosphate homeostasis (*OsPAP3*), and potential stress-related signaling (*PI4Kγ4*) during rice seed development. Additionally, our DEG-myo-Network revealed connections to glycerophosphodiester phosphodiesterases (GDPDs), specifically *OsGDPD2* and *OsGDPD5*, which have been reported to coordinate phosphate and sugar homeostasis (Mehra et al., 2019; Verma et al., 2025).

Further integration of DEGs, module eigengenes correlated with 'myo', and differentially expressed proteins (DEPs) resulted in a DEG-myo-DEP-Network containing 126 genes predominantly associated with nutrient storage and stress tolerance. Within this network, key hub genes included *OsMIPS1*, *OsSSIII*, *OsAlaAT2*, *OsPPDK1*, *protein phosphatase 2C 27*, *OsPHO1;2*, all interconnected to each other. *OsMIPS1* and *OsSSIII* are connected through *OsAlaAT2* and *OsPPDK1*, while *OsSSIII* and *OsPHO1;2* share links with *protein phosphatase 2C 27*. While *OsAlaAT1* has been established as critical for normal starch granule formation in rice endosperm, *OsAlaAT2* is implicated in modulating grain yield by regulating nitrogen use efficiency (Fang et al., 2022; Zhong et al., 2019; Agrawal et al., 2024; Rao et al., 2018). *PPDK* gene governs carbon flux during grain filling and plays a vital role in starch biosynthesis in rice (Kang et al., 2005), as well as nitrogen remobilization (Lin and Wu, 2004). Furthermore, *OsPPDK1* expression is induced under abiotic stresses such as hypoxia and water deficit, underscoring its role in stress adaptation during seed development (Moons et al., 1998). The co-expression of *OsAlaAT2* and *OsPPDK1* alongside *OsMIPS1* and *OsSSIII* suggests their coordinated involvement in PA and starch biosynthesis pathways during grain filling. Furthermore, *OsMIPS1* was directly

connected to 68 genes, predominantly associated with nutrient storage and stress adaptation. These intricate regulatory networks integrate phosphate, nitrogen, and carbon metabolism to coordinate nutrient storage and stress responses during seed development. These identified key genes represent promising targets for future functional characterization, although their precise mechanistic roles require further experimental validation to elucidate their contributions to seed physiology and crop improvement.

4.3. *OsPHR3 coordinates phosphate-carbon partitioning for PA and starch synthesis*

OsPHR3 is known to enhance nitrogen uptake under Pi deficiency, thereby improving nitrogen use efficiency and grain yield (Sun et al., 2018, 2021; Guo et al., 2015). In this study, we provide evidence that *OsPHR3* also plays a central role in phosphate-carbon partitioning, balancing nutrient allocation between starch and phytic acid (PA) biosynthesis during rice seed development. We employed a multiomics systems approach combining transcriptomic, proteomic, and metabolomic datasets, integrated through network-based analysis to derive our results.

Coordinated phosphate-carbon partitioning during seed development is critical for efficient grain filling, nutrient storage, and yield stability. Our DEG-based co-expression network revealed that *OsPHR3* coordinates remobilization of phosphate, sugar and nitrates and other nutrients from the source to the sink organs, by regulating genes such as phosphate transporters (*OsPHO1;1, OsPHO1;3*), sugar transporters (*sugar transport protein MST1, SWEET4*) and nitrate transporters (NRT1/PTR FAMILY 8.3, NRT1/PTR FAMILY 2.11) (Table S6; Fig. 1a; Fig. 8). Nutrient loading into developing grains is a tightly regulated, spatially and temporally dynamic process (Zhang et al., 2007). In rice, most *OsPHR3*-mediated nutrient loading occurs during the early seed-filling phase (up to ~4 DAA). As seed development transition into the mid grain filling stage, most of nutrient reallocation ceases and these genes are downregulated. During this phase, phosphate unloading takes place through *OsPHO1;2* to facilitate nutrient accumulation predominantly as starch through a tightly regulated sucrose, nitrate and carbon fluxes. Genes such as *OsAlaAT2* and *OsPPDK1* play vital role in response to stresses including water deficit, low nitrate and hypoxia (Moons et al., 1998; Fang et al., 2022). During the grain-filling phase, upregulation of *OsMIPS1*, *OsIPK1*, *OsSSIII* and *OsGPT2* was detected in both transcriptomic (DEG) and proteomic (DEP) datasets. *OsMIPS1* and *OsIPK1* are central to PA metabolism (Hitz et al., 2002; Yuan et al., 2007, 2012), while *OsSSIII* and *OsGPT2* are critical for carbon exchange and starch biosynthesis (Toyosawa et al., 2016; Ryoo et al., 2007; Dyson et al., 2014; Weise et al., 2019).

To functionally validate the role of *OsPHR3*, we generated two independent CRISPR/Cas9 knockout lines, *osphr3_ko1* and *osphr3_ko2* (Fig. 5a–d). Loss-of-function of *OsPHR3* led to a marked reduction in the expression of *OsMIPS1*, *OsIPK1*, *OsSSIII* and *OsGPT2,* genes central to phytic acid and starch biosynthesis. The *osphr3* knockout mutant lines, *osphr3_ko1* and osphr*3_ko2* also exhibited a 19.46 and 22.50 % reduction in PA level, respectively, and observed a significant decline in total seed phosphorus. Starch content was also diminished, and scanning electron

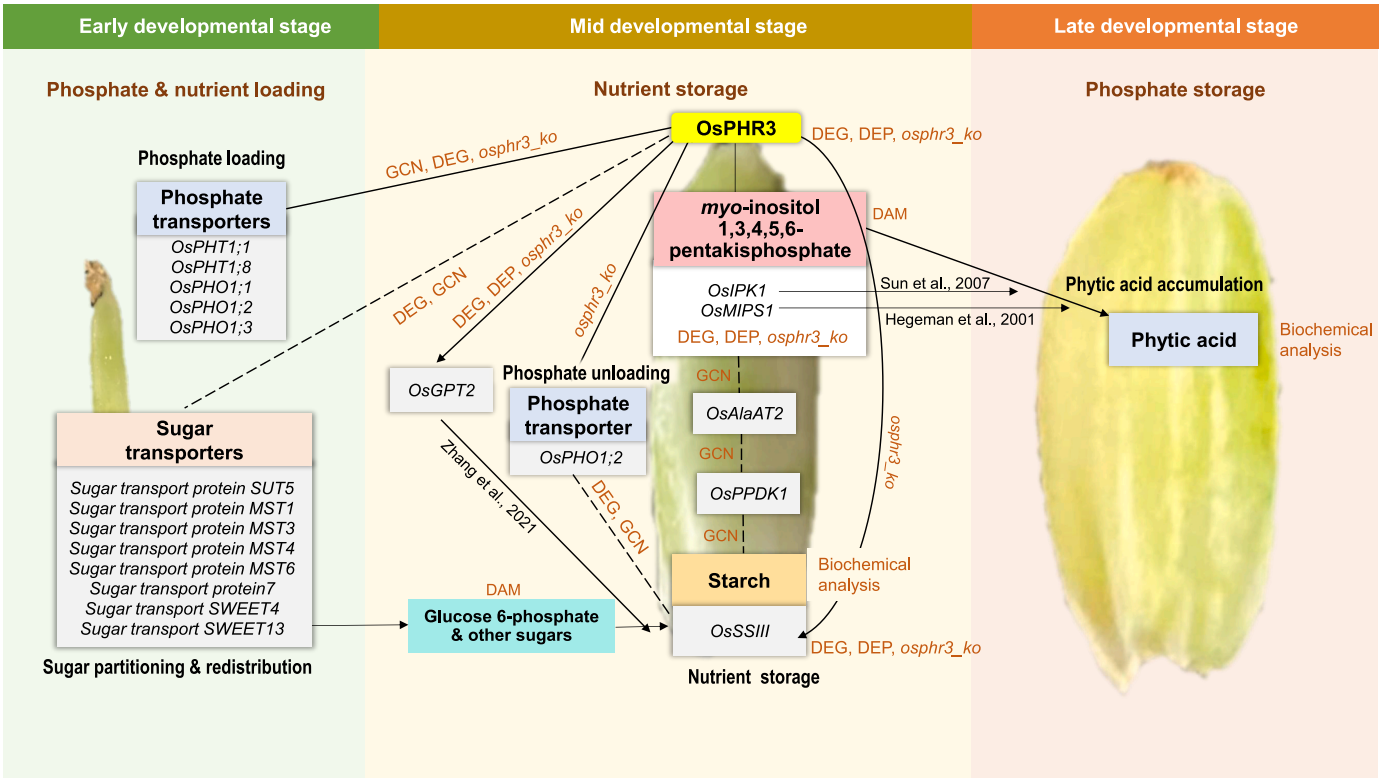

Fig. 8. Schematic overview of *OsPHR3*-centered regulatory network integratng phosphate-carbon reallocation for phytic acid and starch biosynthesis during rice seed development. This working model illustrates how *OsPHR3* coordinates nutrient fluxes early, mid-seed filling and late stages of seed development by integrating transcriptomic, proteomic, and metabolomic data. In the early stage, phosphate and sugars are loaded *via* specific phosphate and sugar transporters. During the mid stage, *OsPHR3* regulates genes involved in starch biosynthesis (*OsSSIII, OsGPT2*) and phytic acid biosynthesis (*OsMIPS1, OsIPK1*) in the late stage. Solid arrows indicate established biochemical routes; dashed arrows represent relationships based on GCN. Genes highlighted are supported by transcriptomic (DEG), proteomic (DEP) and metabolite profiling (DAM), and functional validation. Abbreviations: DEGs, differentially expressed genes; DEP, differentially expressed proteins, GCN, Gene Coexpression Network, *OsPHR3*, *PHOSPHATE STARVATION RESPONSE 3*; *OsIPK1*, *inositol-pentakisphosphate 2-kinase IPK1*; *OsMIPS1*, *myo-inositol-1-phosphate synthase*; *OsAlaAT2*; *alanine-aminotransferase2*, *OsPPDK1*; *pyruvate phosphate dikinase1*, *OsSSIII*; *starch synthase 3*, *OsGPT2*, *glucose-6-phosphate/phosphate translocator 2*.

microscopy revealed irregularly shaped, loosely packed starch granules compared to the densely arranged polyhedral granules in WT. Despite these changes, seed germination and vigor remained comparable to WT (Fig. 5e). These molecular and biochemical alterations were accompanied by pronounced yield penalties, including shorter panicle length, reduced seed dimensions, and lower 100-grain weight, indicating that *OsPHR3* is essential for optimal nutrient accumulation and grain filling.

The observed drop in total seed P is consistent with impaired phosphate mobilization, supported by significantly reduced expression of multiple Pi transporters, including *OsPHO1;1*, *OsPHO1;2*, *OsPHO1;3* *OsPHT1;1* and *OsPHT1;8* genes in mutants (Fig. 7). In our DEG-Network, *OsPHO1;3* is directly connected to *OsPHO1;1*, and both are components of the same transcriptional regulatory network involving *OsPHR3* (Fig. 1b). Impaired starch biosynthesis in mutants aligns with suppressed expression of *OsSSIII, OsPHO1;2* and *OsGPT2*, reinforcing the model that *OsPHR3* integrates phosphate transport with carbon metabolism within a cohesive transcriptional framework (Figs. 7 and 8). These findings highlight the potential role of *OsPHR3* as a central regulator coordinating phosphate mobilization, starch biosynthesis and PA accumulation during rice seed development. *OsPHR3* also showed association with both metabolic and cellular signaling genes, particularly during late developmental stages, points to a dual role in nutrient allocation and stress response modulation. These findings are in consistent with reports that PHR1 transcription factors integrate Pi signaling, metabolic reprogramming, and environmental adaptation (Chan, 2023). Interestingly, the two *OsPHR* homologues, *OsPHR1* and *OsPHR2*, showed significantly higher expression levels in the *osphr3* mutant lines, suggesting that these genes may be partially compensating for the loss of *OsPHR3* function (Fig. S7). This compensatory upregulation likely explains why the seeds remained intact with normal germinability and vigor. These *OsPHR* genes exhibited varied expression across different tissues and developmental stages, indicating a degree of functional diversification. Overexpression of *OsPHR3* conferred significant tolerance to Pi deficiency under field conditions, unlike *OsPHR2* overexpression, making it a potential target for molecular breeding aimed at enhancing PUE and Pi uptake in rice (Guo et al., 2015). Our study demonstrated that knocking out *OsPHR3* reduced phytic acid levels by 19–22 % without detrimental effects on seed formation and germinability, although starch formation was impaired. Based on these findings, we propose that fine-tuning the expression of *OsPHR* homologues offers a promising strategy to balance reduced seed PA content with optimal starch accumulation. These regulatory mechanisms might also be conserved across other crop species, offering valuable targets for higher yields, greater resilience, lower phytate, improved phosphorus use efficiency, and advancing sustainable agriculture.

CRediT authorship contribution statement

Lekha Pazhamala: Writing – original draft, Validation, Methodology, Investigation, Funding acquisition, Formal analysis, Data curation, Conceptualization. **Mandavi Pandey:** Writing – original draft, Visualization, Validation, Methodology, Investigation, Formal analysis, Data curation. **Priyanka Deveshwar:** Writing – review & editing, Methodology, Formal analysis, Data curation. **Arindam Ghatak:** Writing – review & editing, Formal analysis, Data curation. **Wolfram Weckwerth:** Supervision, Resources, Project administration, Funding acquisition. **Palak Chaturvedi:** Writing – review & editing, Investigation, Formal analysis, Data curation. **Jitender Giri:** Writing – review & editing, Validation, Supervision, Resources, Project administration, Funding acquisition, Conceptualization.

Declaration of competing interest

The authors declare that they have no known competing financial interests or personal relationships that could have appeared to influence the work reported in this paper.

Acknowledgements

Lekha T Pazhamala gratefully acknowledges the Department of Biotechnology (DBT), Government of India, for support through the DBT-Research Associateship. Jitender Giri acknowledges funding from the DBT-Indo-Swiss Joint Research Project and the DST-Swarnajayanti Fellowship. The authors thank Lokesh Verma and Bhagat Singh for their valuable assistance in raising the *osphr3* mutants.

Appendix A. Supplementary data

Supplementary data to this article can be found online at https://doi.org/10.1016/j.plaphy.2025.110981.

Data availability

All omics data used in this study are presented in the form of supplementary files. Sequence information of key genes can be accessed in the Rice Annotation Project Database under the following accession numbers: OsPHO1;1 (Os01g0110050), *OsPHO1;2* (Os02g0809800), *OsPHO1;3* (Os06g0493600), *OsPHR3* (Os02g0139000), *OsPHT1;3* (Os10g0444600), *OsGPT2* (Os08g0187800), *OsMIPS1* (Os03g0192700), *OsIPK1* (Os04g0661200); *OsPHT1;8* (Os10g0444700).

References

Agarwal, P., Kapoor, S., Tyagi, A.K., 2011. Transcription factors regulating the progression of monocot and dicot seed development. Bioessays 33, 189–202.
Aggarwal, S., Kumar, A., Bhati, K.K., Kaur, G., Shukla, V.K., Tiwari, S., Pandey, A.K., 2018. RNAi mediated down regulation of inositol penta kisphosphate kinase (IPK1) in wheat grains decreases phytic acid levels and increases Fe and Zn accumulation. Front. Plant Sci. 9, 259.
Agrawal, N., Chunletia, R.S., Badigannavar, A.M., Mondal, S., 2024. Role of alanine aminotransferase in crop resilience to climate change: a critical review. Physiol. Mol. Biol. Plants 30, 1935–1953.
Ali, N., Paul, S., Gayen, D., Sarkar, S.N., Datta, S.K., Datta, K., 2013. RNAi mediated down regulation of myo-inositol-3-phosphate synthase to generate low phytate rice. Rice 6, 1–2.
Alok, A., Singh, S., Kumar, P., Bhati, K.K., 2022. Potential of engineering the myo-inositol oxidation pathway to increase stress resilience in plants. Mol. Biol. Rep. 49, 8025–8035.
Bhadouria, J., Mehra, P., Verma, L., Pazhamala, L.T., Rumi, R., Panchal, P., Sinha, A.K., Giri, J., 2023. Root-expressed rice PAP3b enhances secreted APase activity and helps utilize organic phosphate. Plant Cell Physiol. 64, 501–518.
Bi, J., Liu, Z., Lin, Z., Alim, M.A., Rehmani, M.I., Li, G., Wang, Q., Wang, S., Ding, Y., 2013. Phosphorus accumulation in grains of japonica rice as affected by nitrogen fertilizer. Plant Soil 369, 231–240.
Chan, C., 2023. Coordinating phosphorus and jasmonate signaling: PHR1 partners with transcriptional regulators. Plant Cell 35, 1960–1961.
Che, J., Yamaji, N., Miyaji, T., Mitani-Ueno, N., Kato, Y., Shen, R.F., Ma, J.F., 2020. Node-localized transporters of phosphorus essential for seed development in rice. Plant Cell Physiol. 61, 1387–1398.
Chen, P., Giarola, V., Bartels, D., 2021. The *Craterostigma plantagineum* protein kinase CpWAK1 interacts with pectin and integrates different environmental signals in the cell wall. Planta 253, 1–16.
Chen, S., Zhou, Y., Chen, Y., Gu, J., 2018. Fastp: an ultra-fast all-in-one FASTQ preprocessor. Bioinformatics 34, i884–i890.
Cong, W.F., Suriyagoda, L.D., Lambers, H., 2020. Tightening the phosphorus cycle through phosphorus-efficient crop genotypes. Trends Plant Sci. 25, 967–975.
Conley, D.J., Paerl, H.W., Howarth, R.W., Boesch, D.F., Seitzinger, S.P., Havens, K.E., Lancelot, C., Likens, G.E., 2009. Controlling eutrophication: nitrogen and phosphorus. Science 323, 1014–1015.
Delage, E., Ruelland, E., Guillas, I., Zachowski, A., Puyaubert, J., 2012. Arabidopsis type-III phosphatidylinositol 4-kinases β1 and β2 are upstream of the phospholipase C pathway triggered by cold exposure. Plant Cell Physiol. 53, 565–576.
Dong, J., Yan, W., Bock, C., Nokhrina, K., Keller, W., Georges, F., 2013. Perturbing the metabolic dynamics of myo-inositol in developing Brassica napus seeds through in vivo methylation impacts its utilization as phytate precursor and affects downstream metabolic pathways. BMC Plant Biol. 13, 1–12.
Dien, D.C., Thu, T.T.P., Moe, K., Yamakawa, T., 2019. Proline and carbohydrate metabolism in rice varieties (*Oryza sativa* L.) under various drought and recovery conditions. Plant Physiology Reports 24, 376–387.
Dyson, B.C., Webster, R.E., Johnson, G.N., 2014. GPT2: a glucose 6-phosphate/phosphate translocator with a novel role in the regulation of sugar signalling during seedling development. Ann. Bot. 113, 643–652.

Fang, H., Zhang, Q., Zhang, S., Zhang, T., Pan, F., Cui, Y., Thomsen, S.T., Jakobsen, L.S., Liu, A., Pires, S.M., 2021. Risk–benefit assessment of consumption of rice for adult men in China. Front. Nutr. 8, 694370.

Fang, L.B., Ma, L.Y., Zhao, S.L., Cao, R.J., Jiao, G.A., Hu, P.S., Wei, X.J., 2022. Alanine aminotransferase (*OsAlaAT1*) modulates nitrogen utilization, grain yield, and quality in rice. Journal of Genetics and Genomics 49, 510–513.

Ghatak, A., Chaturvedi, P., Bachmann, G., Valledor, L., Ramšak, Ž., Bazargani, M.M., Bajaj, P., Jegadeesan, S., Li, W., Sun, X., Gruden, K., 2021. Physiological and proteomic signatures reveal mechanisms of superior drought resilience in pearl millet compared to wheat. Front. Plant Sci. 11, 600278.

Gu, M., Chen, A., Sun, S., Xu, G., 2016. Complex regulation of plant phosphate transporters and the gap between molecular mechanisms and practical application: what is missing? Mol. Plant 9, 396–416.

Guo, J., Ling, N., Li, Y., Li, K., Ning, H., Shen, Q., Guo, S., Vandenkoornhuyse, P., 2021. Seed-borne, endospheric and rhizospheric core microbiota as predictors of plant functional traits across rice cultivars dominated by deterministic processes. New Phytol. 230, 2047–2060.

Guo, M., Ruan, W., Li, C., Huang, F., Zeng, M., Liu, Y., Yu, Y., Ding, X., Wu, Y., Wu, Z., Mao, C., Yi, K., Wu, P., Mo, X., 2015. Integrative comparison of the role of the PHOSPHATE RESPONSE1 subfamily in phosphate signaling and homeostasis in rice. Plant Physiol. 168, 1762–1776.

He, Q., Wang, F., Wang, Y., Lu, H., Yang, Z., Lv, Q., Mao, C., 2019. Molecular control and genetic improvement of phosphorus use efficiency in rice. Mol. Breed. 39, 162.

Hitz, W.D., Carlson, T.J., Kerr, P.S., Sebastian, S.A., 2002. Biochemical and molecular characterization of a mutation that confers a decreased raffinosaccharide and phytic acid phenotype on soybean seeds. Plant Physiol. 128, 650–660.

Huang, D.W., Sherman, B.T., Tan, Q., Collins, J.R., Alvord, W.G., Roayaei, J., Stephens, R., Baseler, M.W., Lane, H.C., Lempicki, R.A., 2007. The DAVID gene functional classification tool: a novel biological module-centric algorithm to functionally analyze large gene lists. Genome Biol. 8, 1–16.

Illakwahhi, D.T., Vegi, M.R., Srivastava, B.B., 2024. Phosphorus' future insecurity: the horror of depletion and sustainability measures. Int. J. Environ. Sci. Technol. 21, 9265–9280.

Julia, C., Wissuwa, M., Kretzschmar, T., Jeong, K., Rose, T., 2016. Phosphorus uptake, partitioning and redistribution during grain filling in rice. Ann. Bot. 118, 1151–1162.

Kanehisa, M., Goto, S., 2000. KEGG: kyoto encyclopedia of genes and genomes. Nucleic Acids Res. 28, 27–30.

Kang, H.G., Park, S., Matsuoka, M., An, G., 2005. White-core endosperm floury endosperm-4 in rice is generated by knockout mutations in the C4-type pyruvate orthophosphate dikinase gene (OsPPDKB). Plant J. 42, 901–911.

SPOT-ITN Consortium, Keller, M., Simm, S., 2018. The coupling of transcriptome and proteome adaptation during development and heat stress response of tomato pollen. BMC Genom. 19, 1–20.

Kim, D., Paggi, J.M., Park, C., Bennett, C., Salzberg, S.L., 2019. Graph-based genome alignment and genotyping with HISAT2 and HISAT-Genotype. Nat. Biotechnol. 37, 907–915.

Ko, S.S., Lu, W.C., Hung, J.C., Chang, H.F., Li, M.J., Yeh, K.C., Chiou, T.J., 2024. Maternal effect contributes to grain-filling defects of Ospho1;2 rice mutants. New Phytol. 244, 351–357.

Kruseman, G., Mottaleb, K.A., Tesfaye, K., Bairagi, S., Robertson, R., Mandiaye, D., Frija, A., Gbegbelegbe, S., Alene, A., Prager, S., 2020. Rural transformation and the future of cereal-based agri-food systems. Global Food Secur. 26, 100441.

Kuwano, M., Mimura, T., Takaiwa, F., Yoshida, K.T., 2009. Generation of stable 'low phytic acid'transgenic rice through antisense repression of the 1d-*myo*-inositol 3-phosphate synthase gene (RINO1) using the 18-kDa oleosin promoter. Plant Biotechnol. J. 7, 96–105.

Lambers, H., 2022. Phosphorus acquisition and utilization in plants. Annu. Rev. Plant Biol. 73, 17–42.

Langfelder, P., Horvath, S., 2008. WGCNA: an R package for weighted correlation network analysis. BMC Bioinf. 9, 559.

Leinonen, R., Sugawara, H., Shumway, M., 2010. International nucleotide sequence database collaboration, the sequence read archive. Nucleic Acids Res. 39 (Suppl. l_1), D19–D21.

Li, W.X., Zhao, H.J., Pang, W.Q., Cui, H.R., Poirier, Y., Shu, Q.Y., 2014. Seed-specific silencing of OsMRP5 reduces seed phytic acid and weight in rice. Transgenic Res. 23, 585–599.

Liao, Y., Smyth, G.K., Shi, W., 2014. featureCounts: an efficient general-purpose program for assigning sequence reads to genomic features. Bioinformatics 30, 923–930.

Lin, J.F., Wu, S.H., 2004. Molecular events in senescing arabidopsis leaves. Plant J. 39, 612–628.

Livak, K.J., Schmittgen, T.D., 2001. Analysis of relative gene expression data using real-time quantitative PCR and the 2(-ΔΔCT) method. Methods 25, 402–408.

Lott, J.N.A., Ockenden, I., Raboy, V., Batten, G.D., 2000. Phytic acid and phosphorus in crop seeds and fruits: a global estimate. Seed Sci. Res. 10, 11–33.

Love, M.I., Huber, W., Anders, S., 2014. Moderated estimation of fold change and dispersion for RNA-seq data with DESeq2. Genome Biol. 15, 550. https://doi.org/10.1186/s13059-014-0550-8.

Ma, B., Zhang, L., Gao, Q., Wang, J., Li, X., Wang, H., Liu, Y., Lin, H., Liu, J., Wang, X., Li, Q., Deng, Y., Tang, W., Luan, S., He, Z., 2021. A plasma membrane transporter coordinates phosphate reallocation and grain filling in cereals. Nat. Genet. 53, 906–915.

Ma, B., Zhang, Y., Fan, Y., Zhang, L., Li, X., Zhang, Q.Q., Shu, Q., Huang, J., Chen, G., Li, Q., Gao, Q., Zhu, X.G., He, Z., Wang, P., 2024. Genetic improvement of phosphate-limited photosynthesis for high yield in rice. In: Proceedings of the National Academy of Sciences, vol 121, e2404199121.

Mehra, P., Pandey, B.K., Verma, L., Giri, J., 2017. Improvement in phosphate acquisition and utilization by a secretory purple acid phosphatase (OsPAP21b) in rice. Plant Biotechnol. J. 15, 1054–1067.

Mehra, P., Pandey, B.K., Verma, L., Giri, J., 2019. A novel glycerophosphodiester phosphodiesterase improves phosphate deficiency tolerance in rice. Plant Cell Environ. 42, 1167–1179.

Mohammadi, F., Marti, A., Nayebzadeh, K., Hosseini, S.M., Tajdar-Oranj, B., Jazaeri, S., 2021. Effect of washing, soaking and pH in combination with ultrasound on enzymatic rancidity, phytic acid heavy metals and coliforms of rice bran. Food Chem. 334, 127583.

Moons, A., Valcke, R., Van, M., Montagu, 1998. Low-oxygen stress and water deficit induce cytosolic pyruvate orthophosphate dikinase (PPDK) expression in roots of rice, a C3 plant. Plant J. 15, 89–98.

Pandey, M., Verma, L., Kohli, P.S., Singh, B., Kochi, A., Giri, J., 2024. A lipid synthase maintains metabolic flux for jasmonate synthesis to regulate root growth and phosphate homeostasis. Plant Physiol. kiae453.

Paoletti, A.C., Parmely, T.J., Tomomori-Sato, C., Sato, S., Zhu, D., Conaway, R.C., Conaway, J.W., Florens, L., Washburn, M.P., 2006. Quantitative proteomic analysis of distinct mammalian mediator complexes using normalized spectral abundance factors. In: Proceedings of the National Academy of Sciences, vol 103, pp. 18928–18933.

Pazhamala, L.T., Chaturvedi, P., Bajaj, P., Srikanth, S., Ghatak, A., Chitikineni, A., Bellaire, A., Hingane, A., Kumar, C.S., Saxena, K.B., Weckwerth, W., 2020. Multiomics approach unravels fertility transition in a pigeonpea line for a two-line hybrid system. Plant Genome 13, e20028.

Pazhamala, L.T., Purohit, S., Saxena, R.K., Garg, V., Krishnamurthy, L., Verdier, J., Varshney, R.K., 2017. Gene expression atlas of pigeonpea and its application to gain insights into genes associated with pollen fertility implicated in seed formation. J. Exp. Bot. 68, 2037–2054.

Poirier, Y., Jaskolowski, A., Clúa, J., 2022. Phosphate acquisition and metabolism in plants. Curr. Biol. 32, R623–R629.

Raboy, V., 2001. Seeds for a better future: 'low phytate' grains help to overcome malnutrition and reduce pollution. Trends Plant Sci. 6, 458–462.

Raboy, V., 2003. *myo*-Inositol-1, 2, 3, 4, 5, 6-Hexakisphosphate. Phytochemistry 64, 1033–1043.

Raboy, V., 2007. The ABCs of low-phytate crops. Nat. Biotechnol. 25, 874–875.

Raboy, V., 2009. Approaches and challenges to engineering seed phytate and total phosphorus. Plant Sci. 177, 281–296.

Raboy, V., 2020. Low phytic acid crops: observations based on four decades of research. Plants 9, 140.

Rao, I.S., Neeraja, C.N., Srikanth, B., Subrahmanyam, D., Swamy, K.N., Rajesh, K., Vijayalakshmi, P., Kiran, T.V., Sailaja, N., Revathi, P., Rao, P.R., Rao, L.V.S., Surekha, K., Babu, V.R., Voleti, S.R., 2018. Identification of rice landraces with promising yield and the associated genomic regions under low nitrogen. Sci. Rep. 8, 9200.

Rose, T.J., Liu, L., Wissuwa, M., 2013. Improving phosphorus efficiency in cereal crops: is breeding for reduced grain phosphorus concentration part of the solution? Front. Plant Sci. 4, 444.

Rose, T.J., Rengel, Z., Ma, Q., Bowden, J.W., 2007. Differential accumulation patterns of phosphorus and potassium by canola cultivars compared to wheat. J. Plant Nutr. Soil Sci. 170, 404–411.

Rose, T.J., Welling, M.T., Julia, C.C., Jeong, K., Tong, C., Waters, D.L., Liu, L., 2020. Accumulation of phytate and starch lysophospholipids in rice grains and responses to alterations in P supply or source-sink relations. J. Cereal. Sci. 91, 102896.

Ryoo, N., Yu, C., Park, C.S., Baik, M.Y., Park, I.M., Cho, M.H., Bhoo, S.H., An, G., Hahn, T.R., Jeon, J.S., 2007. Knockout of a starch synthase gene OsSSIIIa/Flo5 causes white-core floury endosperm in rice (*Oryza sativa* L.). Plant Cell Rep. 26, 1083–1095.

Schauer, N., Steinhauser, D., Strelkov, S., Schomburg, D., Allison, G., Moritz, T., Lundgren, K., Roessner-Tunali, U., Forbes, M.G., Willmitzer, L., Fernie, A.R., Kopka, J., 2005. GC-MS libraries for the rapid identification of metabolites in complex biological samples. FEBS (Fed. Eur. Biochem. Soc.) Lett. 579, 1332–1337.

Seck, P.A., Diagne, A., Mohanty, S., Wopereis, M.C., 2012. Crops that feed the world 7: rice. Food Secur. 4, 7–24.

Shannon, P., Markiel, A., Ozier, O., Baliga, N.S., Wang, J.T., Ramage, D., Amin, N., Schwikowski, B., Ideker, T., 2003. Cytoscape: a software environment for integrated models of biomolecular interaction networks. Genome Res. 13, 2498–2504.

Sun, Y., Hu, Z., Wang, X., Shen, X., Hu, S., Yan, Y., Kant, S., Xu, G., Xue, Y., Sun, S., 2021. Overexpression of *OsPHR3* improves growth traits and facilitates nitrogen use efficiency under low phosphate condition. Plant Physiol. Biochem. 166, 712–722.

Sun, Y., Luo, W., Jain, A., Liu, L., Ai, H., Liu, X., Feng, B., Zhang, L., Zhang, Z., Guohua, X., Sun, S., 2018. *OsPHR3* affects the traits governing nitrogen homeostasis in rice. BMC Plant Biol. 18, 1–15.

Toyosawa, Y., Kawagoe, Y., Matsushima, R., Crofts, N., Ogawa, M., Fukuda, M., Kumamaru, T., Okazaki, Y., Kusano, M., Saito, K., Toyooka, K., 2016. Deficiency of starch synthase IIIa and IVb alters starch granule morphology from polyhedral to spherical in rice endosperm. Plant Physiol. 170, 1255–1270.

Tuncel, A., Okita, T.W., 2013. Improving starch yield in cereals by over-expression of ADPglucose pyrophosphorylase: expectations and unanticipated outcomes. Plant Sci. 211, 52–60.

Veneklaas, E.J., Lambers, H., Bragg, J., Finnegan, P.M., Lovelock, C.E., Plaxton, W.C., Price, C.A., Scheible, W.R., Shane, M.W., White, P.J., Raven, J.A., 2012. Opportunities for improving phosphorus-use efficiency in crop plants. New Phytol. 195, 306–320.

Verma, L., Pandey, M., Bhatia, C., Mehra, P., Singh, B., Giri, J., 2025. Phosphate deficiency inducible OsGDPD5 affects root growth by regulating sugar-auxin crosstalk. Plant J. 121, e17249.
Vogiatzaki, E., Baroux, C., Jung, J.Y., Poirier, Y., 2017. PHO1 exports phosphate from the chalazal seed coat to the embryo in developing arabidopsis seeds. Curr. Biol. 27, 2893–2900.
Wang, F., Deng, M., Xu, J., Zhu, X., Mao, C., 2018. Molecular mechanisms of phosphate transport and signaling in higher plants. In: Seminars in Cell & Developmental Biology, vol. 74. Academic Press, pp. 114–122.
Wang, F., Rose, T., Jeong, K., Kretzschmar, T., Wissuwa, M., 2016. The knowns and unknowns of phosphorus loading into grains, and implications for phosphorus efficiency in cropping systems. J. Exp. Bot. 67, 1221–1229.
Wang, L., Cui, J., Zhang, N., Wang, X., Su, J., Vallés, M.P., Wu, S., Yao, W., Chen, X., Chen, D., 2024. *OsIPK1* frameshift mutations disturb phosphorus homeostasis and impair starch synthesis during grain filling in rice. Plant Mol. Biol. 114, 91.
Wang, Y., Wang, F., Lu, H., Liu, Y., Mao, C., 2021. Phosphate uptake and transport in plants: an elaborate regulatory system. Plant Cell Physiol. 62, 564–572.
Weckwerth, W., Ghatak, A., Bellaire, A., Chaturvedi, P., Varshney, R.K., 2020. PANOMICS meets germplasm. Plant Biotechnol. J. 18, 1507–1525.
Weise, S.E., Liu, T., Childs, K.L., Preiser, A.L., Katulski, H.M., Perrin-Porzondek, C., Sharkey, T.D., 2019. Transcriptional regulation of the glucose-6-phosphate/phosphate translocator 2 is related to carbon exchange across the chloroplast envelope. Front. Plant Sci. 10, 460290.
Xie, X., Ma, X., Zhu, Q., Zeng, D., Li, G., Liu, Y.G., 2017. CRISPR-GE: a convenient software toolkit for CRISPR-based genome editing. Mol. Plant 10, 1246–1249.
Xu, L., Yi, K., 2021. Unloading phosphate for starch synthesis in cereal grains. Mol. Plant 14, 1232–1233.
Yamaji, N., Ma, J.F., 2014. The node, a hub for mineral nutrient distribution in graminaceous plants. Trends Plant Sci. 19, 556–563.
Yamaji, N., Ma, J.F., 2017. Node-controlled allocation of mineral elements in Poaceae. Curr. Opin. Plant Biol. 39, 18–24.
Yuan, F.J., Zhu, D.H., Tan, Y.Y., Dong, D.K., Fu, X.J., Zhu, S.L., Li, B.Q., Shu, Q.Y., 2012. Identification and characterization of the soybean IPK1 ortholog of a low phytic acid mutant reveals an exon-excluding splice-site mutation. Theor. Appl. Genet. 125, 1413–1423.
Yuan, F.J., Zhao, H.J., Ren, X.L., Zhu, S.L., Fu, X.J., Shu, Q.Y., 2007. Generation and characterization of two novel low phytate mutations in soybean (*Glycine max* L. Merr.). Theor. Appl. Genet. 115, 945–957.
Zhang, B., Horvath, S., 2005. A general framework for weighted gene co-expression network analysis. Stat. Appl. Genet. Mol. Biol. 4, 1–32.
Zhang, S., Ghatak, A., Bazargani, M.M., Bajaj, P., Varshney, R.K., Chaturvedi, P., Jiang, D., Weckwerth, W., 2021. Spatial distribution of proteins and metabolites in developing wheat grain and their differential regulatory response during the grain filling process. Plant J. 107, 669–687.
Zhang, S., Ghatak, A., Mohammadi Bazargani, M., Kramml, H., Zang, F., Gao, S., Ramšak, Ž., Gruden, K., Varshney, R.K., Jiang, D., Chaturvedi, P., 2024. Cell-type proteomic and metabolomic resolution of early and late grain filling stages of wheat endosperm. Plant Biotechnol. J. 22, 555–571.
Zhang, W.H., Zhou, Y., Dibley, K.E., Tyerman, S.D., Furbank, R.T., Patrick, J.W., 2007. Nutrient loading of developing seeds. Funct. Plant Biol. 34, 314–331.
Zhang, Z., Huo, W., Wang, X., Ren, Z., Zhao, J., Liu, Y., He, K., Zhang, F., Li, W., Jin, S., Yang, D., 2023. Origin, evolution, and diversification of the wall-associated kinase gene family in plants. Plant Cell Rep. 42, 1891–1906. https://doi.org/10.1007/s00299-023-03068-9.
Zheng, X., Lim, P.K., Mutwil, M., Wang, Y., 2024. A method for mining condition-specific co-expressed genes in Camellia sinensis based on k-means clustering. BMC Plant Biol. 24, 373.
Zhong, M., Liu, X., Liu, F., Ren, Y., Wang, Y., Zhu, J., Teng, X., Duan, E., Wang, F., Zhang, H., Wu, M., 2019. FLOURY ENDOSPERM12 encoding alanine aminotransferase 1 regulates carbon and nitrogen metabolism in rice. J. Plant Biol. 62, 61–73.